









Dedifferentiation-derived neural stem cells exhibit perturbed temporal progression

Kellie Veen^{1,2,3} , Phuong-Khanh Nguyen^{1,2} , Francesca Froidi^{1,2}, Qian Dong^{1,2} ,
Edel Alvarez-Ochoa^{1,2} , Kieran F Harvey^{1,2,4}, John PD McMullen⁵ , Owen Marshall^{5,†} ,
Patricia R Jusuf^{3,†}  & Louise Y Cheng^{1,2,6,*} 

Abstract

Dedifferentiation is the reversion of mature cells to a stem cell-like fate, whereby gene expression programs are altered and genes associated with multipotency are (re)expressed. Misexpression of multipotency factors and pathways causes the formation of ectopic neural stem cells (NSCs). Whether dedifferentiated NSCs faithfully produce the correct number and types of progeny, or undergo timely terminal differentiation, has not been assessed. Here, we show that ectopic NSCs induced via bHLH transcription factor Deadpan (Dpn) expression fail to undergo appropriate temporal progression by constantly expressing mid-temporal transcription factor(tTF), Sloppy-paired 1/2 (Slp). Consequently, this resulted in impaired terminal differentiation and generated an excess of Twin of eyeless (Toy)-positive neurons at the expense of Reversed polarity (Repo)-positive glial cells. Preference for a mid-temporal fate in these ectopic NSCs is concordant with an enriched binding of Dpn at mid-tTF loci and a depletion of Dpn binding at early- and late-tTF loci. Retriggering the temporal series via manipulation of the temporal series or cell cycle is sufficient to reinstate neuronal diversity and timely termination.

Keywords dedifferentiation; *Drosophila*; neuroblast; temporal transcription factors; terminal differentiation

Subject Categories Development; Neuroscience; Stem Cells & Regenerative Medicine

DOI 10.15252/embr.202255837 | Received 22 July 2022 | Revised 6 March 2023 | Accepted 20 March 2023 | Published online 11 April 2023

EMBO Reports (2023) 24: e55837

Introduction

The central nervous system (CNS) is the cognitive control centre of the body and is generated by neural stem cells (NSCs) during

development. *Drosophila* NSCs, called neuroblasts (NBs), exhibit key properties of mammalian NSCs such as self-renewal, temporal control of proliferation and production of different neural subtypes that will form the adult brain. Thus, NBs serve as a powerful model to study the mechanisms that underlie the determination of overall brain size and neuronal diversity (Harding & White, 2018).

Molecular differences such as the mode of division and the temporal identity exist between different NB populations located in different parts of the brain. NBs within the ventral nerve cord (VNC) and the central brain (CB) of the larval CNS undergo Type I divisions, whereby the NB divides asymmetrically to generate a NB and a smaller ganglion mother cell (GMC). The GMC then divides to produce two daughter cells, which terminally differentiate into neurons or glia. A subset of NBs in the larval CB undergo Type II division, in which the NB's asymmetric division generates a NB and an intermediate neural progenitor (INP). Intermediate neural progenitors mature prior to dividing asymmetrically to produce another progenitor and a GMC. Within the optic lobes (OLs), the medulla outer proliferation centre (OPC) NBs are formed from a pseudostratified neuroepithelium through a differentiation wave characterised by proneural factor expression, termed the “proneural wave” (Egger *et al*, 2007; Yasugi *et al*, 2008). These NBs undergo asymmetric division and are broadly thought to behave similarly to Type I NBs.

In addition to positional identity, NBs can also be temporally defined by the expression pattern of sequential markers, known as the temporal series or temporal transcription factors (tTFs). The tTFs confer temporal identity to neurons born within each tTF window, and their cross-regulation ensures unidirectional progression through the temporal series (Li *et al*, 2013; Suzuki *et al*, 2013). Type I, II and medulla NBs all express unique sets of tTFs; however, in all the regions of the CNS, tTFs play conserved roles to control neuronal diversity and proliferative potential of NBs (Maurange *et al*, 2008; Bayraktar & Doe, 2013; Li *et al*, 2013; Suzuki *et al*, 2013; Eroglu *et al*, 2014; Liu *et al*, 2015; Ren *et al*, 2017; Syed *et al*, 2017;

1 Peter MacCallum Cancer Centre, Melbourne, VIC, Australia

2 Sir Peter MacCallum Department of Oncology, The University of Melbourne, Melbourne, VIC, Australia

3 School of Biosciences, The University of Melbourne, Melbourne, VIC, Australia

4 Department of Anatomy and Developmental Biology, Monash University, Clayton, VIC, Australia

5 Menzies Institute for Medical Research, Medical Science Precinct, Hobart, TAS, Australia

6 Department of Anatomy and Physiology, The University of Melbourne, Melbourne, VIC, Australia

*Corresponding author. Tel: +61 450053363; E-mail: louise.cheng@petermac.org

†These authors contributed equally to this work as senior authors

Abdusselamoglu *et al*, 2019; Pahl *et al*, 2019; Konstantinides *et al*, 2022; Zhu *et al*, 2022).

One of the key regulatory mechanisms of brain size and neuronal diversity is the control of neuronal cell fate maintenance. We and others have shown that a number of transcription factors including Longitudinals Lacking (Lola), Midlife crisis and Nervous fingers 1 (Nerfin-1) prevent neuron-to-NB reversion by repressing the expression of NB and cell-cycle genes in post-mitotic neurons in the OLs (Carney *et al*, 2013; Southall *et al*, 2014; Froidi *et al*, 2015, 2019; Xu *et al*, 2017; Vissers *et al*, 2018). Additionally, signalling pathways such as Notch can influence the differentiation status of neurons as expression of hyperactivated Notch can induce neuronal dedifferentiation and the formation of ectopic NBs (Xu *et al*, 2017; Vissers *et al*, 2018). However, the molecular mechanisms by which these factors regulate neuronal fate is not well-understood. This is important for defining the logic by which NSCs mature into neurons and what prevents them from reverting into NSCs. Such knowledge is necessary for understanding normal CNS development, as well as in disease settings such as cancer. Furthermore, it could potentially be harnessed to promote regeneration. In this study, we identified the basic helix–loop–helix (bHLH) transcription factor, Deadpan (Dpn), as a mediator of dedifferentiation downstream of Nerfin-1 in the OL. Overexpression of Dpn caused the formation of supernumerary NBs in deep neuronal layers of the medulla. The dedifferentiated NBs acquired and maintained an Eyeless (Ey)/Sloppy paired (Slp)-positive mid-temporal identity throughout larval neurogenesis, delaying the onset of the late-tTF Tailless (Tll)-positive fate. As a result, excessive Twin of eyeless (Toy)-positive progeny was made at the expense of Tll-positive neurons and Reversed polarity (Repo) glial cells. Furthermore, ectopic NBs generated via Dpn overexpression underwent slower cell cycle progression, and failed to terminally differentiate in a timely fashion. Mechanistically, our DamID analysis showed that Dpn binds preferentially to the mid-temporal tTFs, where we observed a depletion of Dpn binding at early- and late-tTF loci. Furthermore, retriggering the progression of the tTFs via Dichaete (D) was able to rescue both neuronal diversity and terminal differentiation. Similarly, promoting NB progression through G1/S phase of the cell cycle was able to restore temporal progression, neuronal diversity and terminal differentiation. Finally, we show that dedifferentiation induced by inhibition of Lola, Nerfin-1, as well as hyperactivation of Notch in the OL similarly caused stalled temporal progression.

Together, our findings suggest that cell cycle regulators and temporal transcription factors are key determinants of proliferation and termination profiles of dedifferentiated NBs. To utilise dedifferentiated NSCs for regenerative purposes, we will have to recreate the correct temporal profiles and ensure cell cycle progression occurs appropriately.

Results

Deadpan overexpression induces ectopic neuroblasts in the optic lobe medulla region

We and others have previously shown that the Nerfin-1 transcription factor maintains neuronal differentiation in Type I, II and medulla neuronal lineages (Froidi *et al*, 2015; Xu *et al*, 2017; Vissers

et al, 2018). In the absence of Nerfin-1, neurons undergo dedifferentiation to acquire a NB-like fate, by turning on bona-fide NB markers such as Deadpan (Dpn) and Miranda (Mira; Froidi *et al*, 2015; Xu *et al*, 2017; Vissers *et al*, 2018). In the OLs, symmetrically dividing neuroepithelial cells differentiate into medulla NBs located at the superficial CNS surface (0 μm , Fig 1A and B, pink), which in turn generates medulla neurons that occupy the deep layers of the CNS at around 8–12 μm from the superficial surface (Fig 1A–C, green; Egger *et al*, 2007; Yasugi *et al*, 2008). The pan-neural bHLH transcription factor, Dpn, lies downstream of Notch signalling (San-Juán & Baonza, 2011; San-Juán *et al*, 2012) and was identified to be a Nerfin-1 target gene in our previous DamID analyses (Vissers *et al*, 2018). To assess whether Dpn lies functionally downstream of Nerfin-1, we tested whether *UAS-dpn* caused neuronal dedifferentiation. Using three different neuronal/NB drivers (See Fig EV1 and methods for detailed expression analysis of the *GAL4s*) – *GMR31H08-GAL4* (Jenett *et al*, 2012), *ey^{OK107}-GAL4* (Morante *et al*, 2011) and *eyR16F10-GAL4* (Jenett *et al*, 2012), we found that Dpn overexpression in the medulla region of the brain induced the formation of ectopic NBs in deep sections of the CNS (Fig EV1A and B, G and H, and M and N, Vissers *et al*, 2018). Further confirmation of dedifferentiation was made through temporally restricted expression of Dpn during L3 using *GAL80ts;GMR31H08-GAL4*. In this scenario, transgene expression in mature neurons also induced dedifferentiation (Fig EV1C and D). Finally, we confirmed that Dpn overexpression is capable of inducing neuronal dedifferentiation using clonal analysis (Fig 1D, via heat shock-induced *actin-Gal4 flip-out*). Ectopic NBs (Mira⁺) were first recovered in clones 24 h after heat shock (AHS) in deep sections of the CNS (Fig 1F–I, quantified in Fig 1E). This demonstrates that wild-type NBs first generated mature neurons (indicated by the lack of ectopic NBs at 16 h AHS), which then underwent dedifferentiation to give rise to ectopic NBs by 24 h AHS. These ectopic NBs failed to express the neuronal marker Elav (Appendix Fig S1B–B’), and actively divided, as indicated by the M-phase marker phospho-Histone H3 (pH3, Appendix Fig S1A–A’). By 72 h AHS, clones that overexpressed Dpn possessed multiple Mira⁺ cells (Fig 1J and K).

As Dpn was identified to be a target of Nerfin-1, we next investigated the epistatic relationship between Dpn and Nerfin-1. We induced clones expressing Nerfin-1 RNAi and compared the level of dedifferentiation with that of Nerfin-1 RNAi clones additionally expressing Dpn RNAi. We found that Dpn RNAi expression significantly reduced the number of ectopic NBs induced by Nerfin-1 knockdown, suggesting that Dpn lies downstream of Nerfin-1 to mediate neuronal cell fate maintenance (Appendix Fig S1C–F).

Ectopic neuroblasts generated via Dpn overexpression express mid-temporal transcription factors

NBs contribute to the sequential generation of different neuron types by changing the expression of temporal transcription factors (tTFs) in a defined sequence (Apitz & Salecker, 2014). In the OLs, medulla NBs sequentially express a series of tTFs including the early factor Homothorax (Hth), mid-tTFs Eyeless (Ey), Sloppy paired 1/2 (Slp) and Dichaete (D), and late-tTF Tailless (Tll; Li *et al*, 2013; Suzuki *et al*, 2013). The tTFs contribute to the progression of the temporal series by activating the next tTF while repressing the previous tTF (Fig 2A). Medulla NBs continuously

transit through the temporal cascade as they age; therefore, at any given time, different NBs in the superficial layer of the medulla would express Hth, Ey, Slp, D, Tll or a combination of these tTFs

(Fig 2C–G'). As expected, 72 h after clone induction (Fig 2B), about 20–30% the superficial NBs were positive for either Hth, Ey, Slp, D or Tll (or a combination of these factors, Fig 2M).

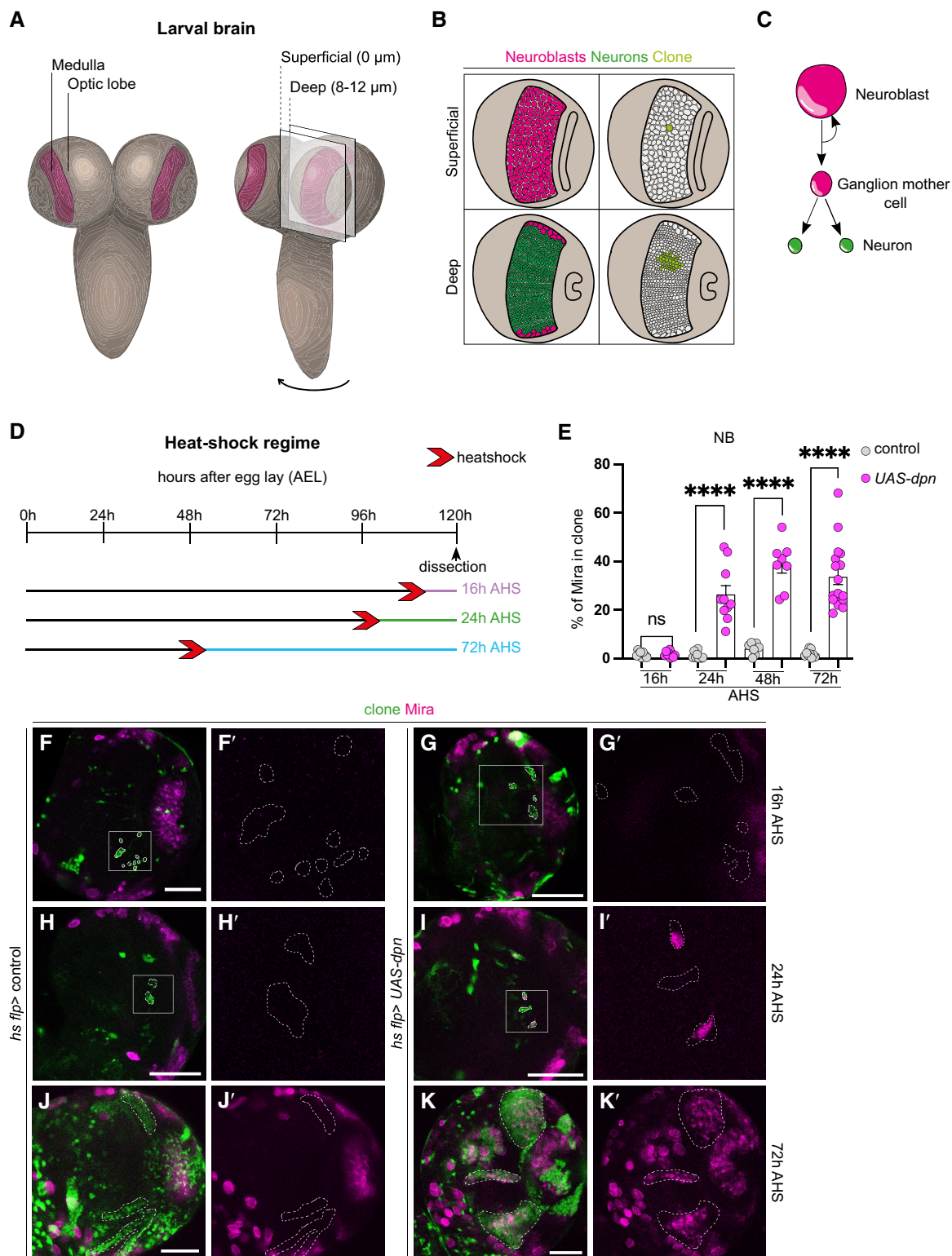


Figure 1.

Figure 1. Dpn overexpression causes reversion of neurons to NBs in the deep layers of the developing CNS.

- A Schematic representation of the larval central nervous system (CNS). Medulla (depicted in maroon) is located with the optic lobes (OLs) of the CNS. Cross section and cell composition at superficial surface (0 μm) and deep layer (8–12 μm) of the OLs are depicted in (B).
- B (left) Superficial surface is occupied by neuroblasts (NBs, pink), and deep layers are occupied by neurons (green). (right) Cross section through a *hs flp* clone (light green) showing the clone consists of a single NB in the superficial layer and its neuronal progeny in the deep layer.
- C Schematic representation of NB divisions: NBs undergo asymmetric division to give rise to a Ganglion mother cell (GMC) that produces two neurons.
- D Schematic depicting the heat shock regimes used in (E–K). Clones were induced via heat shock (red arrows), and dissected at 16 h (purple), 24 h (green), and 72 h (blue) after heat shock.
- E Quantification of % *Mira*⁺ cells in control and *UAS-dpn* clones (calculated as the ratio of *Mira*⁺ cell volume as a percentage of total clone volume). Sixteen hours (Control $n = 9$, $m = 1.584 \pm 0.3779$, *UAS-dpn* $n = 9$, $m = 1.657 \pm 0.37$), 24 h (Control $n = 9$, $m = 1.150 \pm 0.4781$, *UAS-dpn* $n = 10$, $m = 26.37 \pm 3.629$), 48 h (Control $n = 7$, $m = 3.971 \pm 0.9249$, *UAS-dpn* $n = 8$, $m = 38.56 \pm 3.446$), 72 h (Control $n = 9$, $m = 1.874 \pm 0.4897$, *UAS-dpn* $n = 17$, $m = 33.62 \pm 3.243$).
- F–K' (F', G', H', I') are the magnified images of the square region outlined in (F, G, H, I). (F–K) are merged images, (F'–K') are single channel images of (F–K) depicting the presence of NBs (*Mira*⁺). Clones (green) are outlined by dotted lines. All images in this figure, and all following figures are single confocal sections. (F–F' and G–G') No *Mira*⁺ NBs are recovered in deep sections of control or *UAS-dpn* clones at 16 h after clone induction. Quantified in (E). (H–H' and I–I') At 24 h after clone induction, *Mira*⁺ NBs are recovered in *UAS-dpn* but not control clones. Quantified in (E). (J–J' and K–K') At 72 h after clone induction, numerous *Mira*⁺ NBs are recovered in *UAS-dpn* but not in control clones. Quantified in (E).

Data information: Data are represented as mean \pm SEM. *P*-values were obtained using unpaired *t*-test, and Welch's correction was applied in case of unequal variances. *****p* < 0.0001. Scale bars: 50 μm .

Surprisingly, the ectopic NBs in *UAS-dpn* clones mostly expressed the mid-tTFs *Ey* and *Slp* (Fig 2I–J' and M), while some ectopic NBs expressed *D* and very few expressed the early-tTF *Hth* or the late-tTF *Tll* (Fig 2H–H', K–L' and M).

As NBs age, they are expected to undergo sequential transition through the sequence of *Hth* \rightarrow *Ey* \rightarrow *Slp* \rightarrow *D* \rightarrow *Tll* tTFs (Li *et al*, 2013; Suzuki *et al*, 2013). To assess whether ectopic NBs induced via *Dpn* overexpression also underwent sequential expression of these transcription factors, we induced *UAS-dpn* clones, and examined their temporal profile at 24, 48, 72 and 96 h AHS (Fig 3A–F', H–H' and J–J'). At all time points examined, we found that between 40 and 70% of the dedifferentiated NBs expressed *Slp* (used as a proxy for midtemporal identity as it is specifically expressed in the NBs and not in neurons; Fig 3B). In addition, only 5% of the ectopic NBs generated via *Dpn* overexpression were positive for the late-tTF *Tll* at 96 h AHS, compared to ~50% of control NBs at the same time (Fig 3G–K). Together, this indicates that ectopic NBs induced by *Dpn* overexpression adopt a mid-temporal identity shortly after clone induction and maintain this identity throughout larval development.

Neuroblasts generated via *Dpn* overexpression exhibit delayed terminal differentiation

Medulla NBs progress through the series of temporal factors until the oldest medulla NBs express Glial cells missing (*Gcm*) and transition from neurogenesis to gliogenesis and exit the cell cycle (Li *et al*, 2013; preprint: Zhu *et al*, 2021). Medulla NB cell cycle exit occurred around 16 h after pupal formation (APF) in control OLs (29°C, Fig 4A–D and J, no *Mira*⁺ NBs are recovered at this time point). When *Dpn* was overexpressed with *eyR16F10-GAL4* (Jenett *et al*, 2012), which strongly drives gene expression in the pupal CNS (Fig EV1Q and R), significantly more NBs were recovered at 16 h, indicating that NBs termination was delayed (Fig 4H and J). *UAS-dpn* NBs maintained the expression of the mid-tTF *Slp* until at least 10 h APF (Fig EV2A–C", E and F–G"), but prior to their terminal differentiation they began to reduce *Slp* expression and expressed the late-tTF *Tll* (Fig EV2D and E). These data suggest that ectopic NBs generated via *Dpn* overexpression exhibit a prolonged mid-temporal identity before eventually switching on late-tTFs, and undergoing

terminal differentiation and exiting the cell cycle, as no NBs were detected by 24 h APF (Fig 4E–J).

Dpn overexpression induces neuroblasts to generate *Toy*⁺ progeny at the expense of *Tll*⁺ neurons and *Repo*⁺ glial cells

Hth, *Ey*, *Slp*, *D* and *Tll* are each required for the sequential generation of different medulla neurons through the production of Brain-specific homeobox (*Bsh*), Drifter (*Dfr*), *Toy/Sox102F*, *Ets* at 65A (*Ets65a*) and *Tll*, respectively (Morante & Desplan, 2008; Hasegawa *et al*, 2011; Li *et al*, 2013; Suzuki *et al*, 2013; Fig 4N). We next assessed the neuronal subtypes made by *Dpn*-induced ectopic NBs. To better assess the cumulative effect of the neurons that are made throughout CNS development, *ey^{OK107}-GAL4* was used to drive the expression of *Dpn*. About 50% more *Toy*⁺ progeny were made by *Dpn*-induced ectopic NBs than by control NBs (Fig 4K–M). Consistent with this, *UAS-dpn* clones produced very few *Tll*⁺ neurons or *Repo*⁺ glial cells (Fig 4O–T). This indicates that *Dpn* overexpression in the medulla stalls the temporal progression of NBs, causing them to produce an excess of *Toy*⁺ progeny at the expense of *Tll*⁺ neurons and *Repo*⁺ glial cells.

Genome-wide profiling of *Dpn* binding reveals a bias towards mid-temporal identity genes in medulla neuroblasts

To understand why NBs dedifferentiated from medulla neurons specifically adopt a mid-temporal fate, we profiled the genome-wide binding of *Dpn* in 3rd instar larval NBs using Targeted DamID (TaDa; Southall *et al*, 2013; Marshall *et al*, 2016). Using the NB-specific *wor-GAL4* driver line, and a *Dpn*-Dam profiling line generated via FlyORF-TaDa (Aughey *et al*, 2021), we profiled the binding sites of *Dpn* in all larval NBs. We then compared this to the binding of *Dpn* profiled only in medulla NBs, obtained using the NanoDam technique (Tang *et al*, 2022), a BAC-recombined *Dpn*-GFP line under endogenous control, and the medulla-specific *eyR16F10-GAL4* driver line. We found that although *Dpn* bound in proximity to all five temporal cascade TFs in all NBs (Fig 5A–E and G), the binding of *Dpn* was lost or significantly reduced at *hth* and *tll* in medulla NBs, and

significantly increased at *ey* and *slp1* (Fig 5F). Extending this analysis to the recently described complete medulla temporal patterning TF network (Zhu et al, 2022) showed a significant

enrichment of Dpn binding at almost all mid-temporal identity TFs, and a significant depletion at early and late tTFs (Figs EV3A and EV4A–C). Collectively, our genomics and genetic data

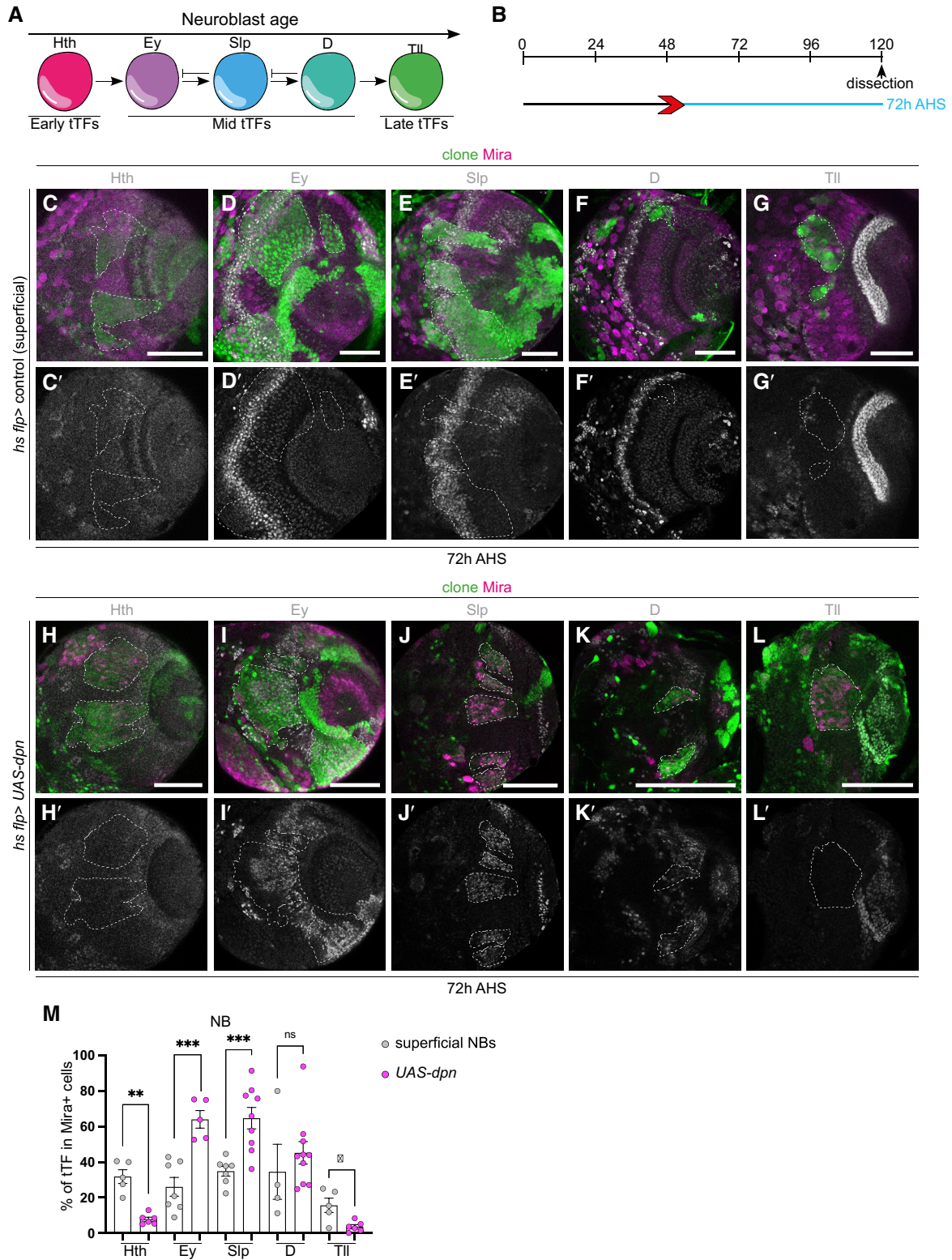


Figure 2.

Figure 2. Ectopic NBs generated via *dpn* overexpression express mid-temporal transcription factors.

- A Schematic representation of temporal series in neuroblasts (NBs). NBs express temporal transcription factors (tTFs; Hth, Ey, Slp, D, Tll) as they age. These can be categorised into early, mid, and late tTFs.
- B Schematic depicting the heat shock regimes used in (C–L'). Clones were induced via heat shock (red arrows) and dissected at 72 h (blue) after heat shock.
- C–L' Representative images of the deep medulla neuronal layer or NB superficial layer in the larval optic lobe, in which *UAS-dpn* or control are driven in clones by *hs flp* (marked by GFP and outlined) and stained with the stem cell marker, Miranda (Mira, magenta), and various temporal transcription factors (tTFs) (grey). (C–C') In superficial sections of control clones, Mira⁺ superficial NBs express the tTF: Hth, Ey, Slp, D, Tll in concentric patterns. Quantified in (M). (H–L') In deep sections of the NB clone induced via *UAS-dpn*, Mira⁺ NBs do not express early tTF Hth or late-tTF Tll, but are positive for mid-tTFs Ey, Slp and D. Quantified in (M).
- M Quantification of volume of cells that express a specific tTF as % of total Mira⁺ NB volume within a clone. Hth (Control $n = 5$, $m = 31.86 \pm 3.89$, *UAS-dpn* $n = 6$, $m = 7.779 \pm 1.212$), Ey (Control $n = 7$, $m = 26.05 \pm 5.302$, *UAS-dpn* $n = 5$, $m = 64.08 \pm 4.936$), Slp (Control $n = 7$, $m = 34.87 \pm 2.753$, *UAS-dpn* $n = 9$, $m = 64.72 \pm 6.045$), D (Control $n = 4$, $m = 34.57 \pm 15.49$, *UAS-dpn* $n = 10$, $m = 45.2 \pm 6.339$), Tll (Control, $n = 5$, $m = 15.65 \pm 4.036$, *UAS-dpn* $n = 6$, $m = 3.584$, ± 1.87).
- Data information: Data are represented as mean \pm SEM. P-values were obtained performing unpaired t-test, and Welch's correction was applied in case of unequal variances. *** $P < 0.001$, ** $P < 0.005$, * $P < 0.05$. Scale bars: 50 μ m.

suggest that the mid-temporal identity tTFs are direct targets of Dpn in the medulla and are activated upon Dpn overexpression.

Dichaete triggers the re-initiation of the temporal series

The mid-temporal identity tTFs form a mutually exclusive regulatory network, where the expression of one inhibits the others (Li *et al*, 2013; Suzuki *et al*, 2013; Zhu *et al*, 2022). Consistent with this, we found that D and Slp were expressed in a complementary pattern in *UAS-Dpn* clones, where high expression of D correlated with low expression of Slp (Fig EV3B–D''', closed arrows), and vice versa (Fig EV3B–D''', open arrows). Next, we investigated whether inhibiting Slp expression via overexpression of D was sufficient to promote temporal progression in stalled Dpn-overexpressing NBs. Overexpression of D in *UAS-dpn* clones caused a significant reduction in Slp expression, and a corresponding increase in Tll expression in NBs, indicating that D can promote NB temporal progression towards a late temporal identity (Fig 6A–B'', F and I). This also induced an increase in the production of Tll⁺ neurons and Repo⁺ glial cells (Fig 6G–H'', J and K), indicating that D promoted NB temporal progression towards a late temporal fate. While a reduction in Toy⁺ progeny was also observed (Fig 6C–E'), this reduction was not significant, as neurons produced by D⁺ NBs can also express Toy (Bertet *et al*, 2014). Consistent with the model that D causes premature termination of the neurogenesis programme, we found that D overexpression in *UAS-dpn* NBs did not increase cell death (Fig EV3E–G), but an earlier cessation of neurogenesis, as indicated by a reduction in Mira⁺ cells at 6 h APF (*eyR16F10-GAL4* (Fig 6L–N), flip-out clones (Fig EV3H–J)).

Temporal progression of dedifferentiated neuroblasts is regulated by the cell cycle

Cell division is essential for neurogenesis, and the progression through the cell cycle is important for temporal transition in Type I NBs (van den Amelee & Brand, 2019). We performed an EdU pulse chase experiment, which showed that *UAS-dpn* clones produced significantly fewer progeny compared with control clones (the number of EdU⁺ cells was normalised to the number of NBs), suggesting that the pace of the cell cycle was slower in dedifferentiated NBs compared with wild-type NBs (Fig 7A–B'', D and E). In addition, our DamID analysis showed that the cell cycle genes *cyclin D* (*cycD*), *cyclin E* (*cycE*) and *string* (*stg*) are direct targets of

Dpn (Fig EV4D–F). Therefore, it is possible that Dpn can directly inhibit cell cycle progression, which in turn prevents temporal transition. To test this hypothesis, we overexpressed the key cell cycle regulators E2F transcription factor 1 (E2f1) and CycE, which can promote cell cycle progression at both the G2/M and G1/S check points (Fig 7L). This manipulation induced a small increase in Mira⁺ NBs (Fig 7G–I) and was able to promote temporal progression in Dpn-expressing NBs, as indicated by fewer Slp⁺ NBs and a significant increase in Repo⁺ glial cells (Fig 7G–H'', J and K).

Interestingly, overexpression of CycD and Cyclin-dependent kinase 4 (Cdk4), which promotes G1/S progression (Fig 7L), had an even stronger effect on temporal transition, resulting in premature neurogenesis (Appendix Fig S2B–D) to gliogenesis (Appendix Fig S2E–G) at 96h AEL. As both D and cell cycle genes can promote temporal progression in *UAS-dpn* clones, we next assessed whether *UAS-D* also affected cell cycle progression in *UAS-dpn* clones. By performing an EdU pulse chase assay, we found that D overexpression did not significantly increase the rate of neuronal production in dedifferentiated NBs (Fig 7C–C'' and F). Together, this data suggest that in the OL, cell cycle progression lies upstream of the temporal series, to promote the generation of neurons.

Notch, Lola and Nerfin-1-mediated dedifferentiation also causes temporal series progression defects

To determine whether dedifferentiated NBs commonly exhibit defects in their temporal identity, we next examined other models of neuronal dedifferentiation. Notch (N) lies upstream of Dpn (San-Juán & Baonza, 2011) and is a Nerfin-1 target gene. N activation phenocopied loss of Nerfin-1, resulting in neuron to NB dedifferentiation (Vissers *et al*, 2018; Fig 8A–E). Furthermore, it was recently shown that the N pathway regulates Slp1 and Slp2 expression in medulla NBs through direct binding to Slp1/2 enhancers (preprint: Ray & Li, 2021). To test whether N activation, such as Dpn overexpression, stalled tTF progression, we assessed Slp expression in medulla regions where *UAS-N^{ACT}* was expressed under the control of *eyR16F10-GAL4*. We found that the ectopic NBs induced via N^{ACT} exhibited significantly increased expression of the mid-tTF Slp (Fig 8C–C'' and F), and resulted in an increase in the number of Toy⁺ neurons (Fig 8I–J'). Similar to Dpn overexpression, dedifferentiated NBs caused by N activation failed to undergo timely terminal cell cycle exit. At 24 h APF, when all wild-type NBs have exited the

cell cycle, NBs generated via N^{ACT} continued to persist (Appendix Fig S2A and H). Next, we asked whether overexpression of D, known to repress Slp, could re-initiate temporal progression, restore neuronal progeny composition and complete timely terminal

differentiation in Notch-mediated dedifferentiation. Overexpression of D did not significantly affect the rate of dedifferentiation (Fig 8E), but significantly increased the proportion of NBs that expressed the late-tTF Tll and reduced the proportion of NBs that expressed the

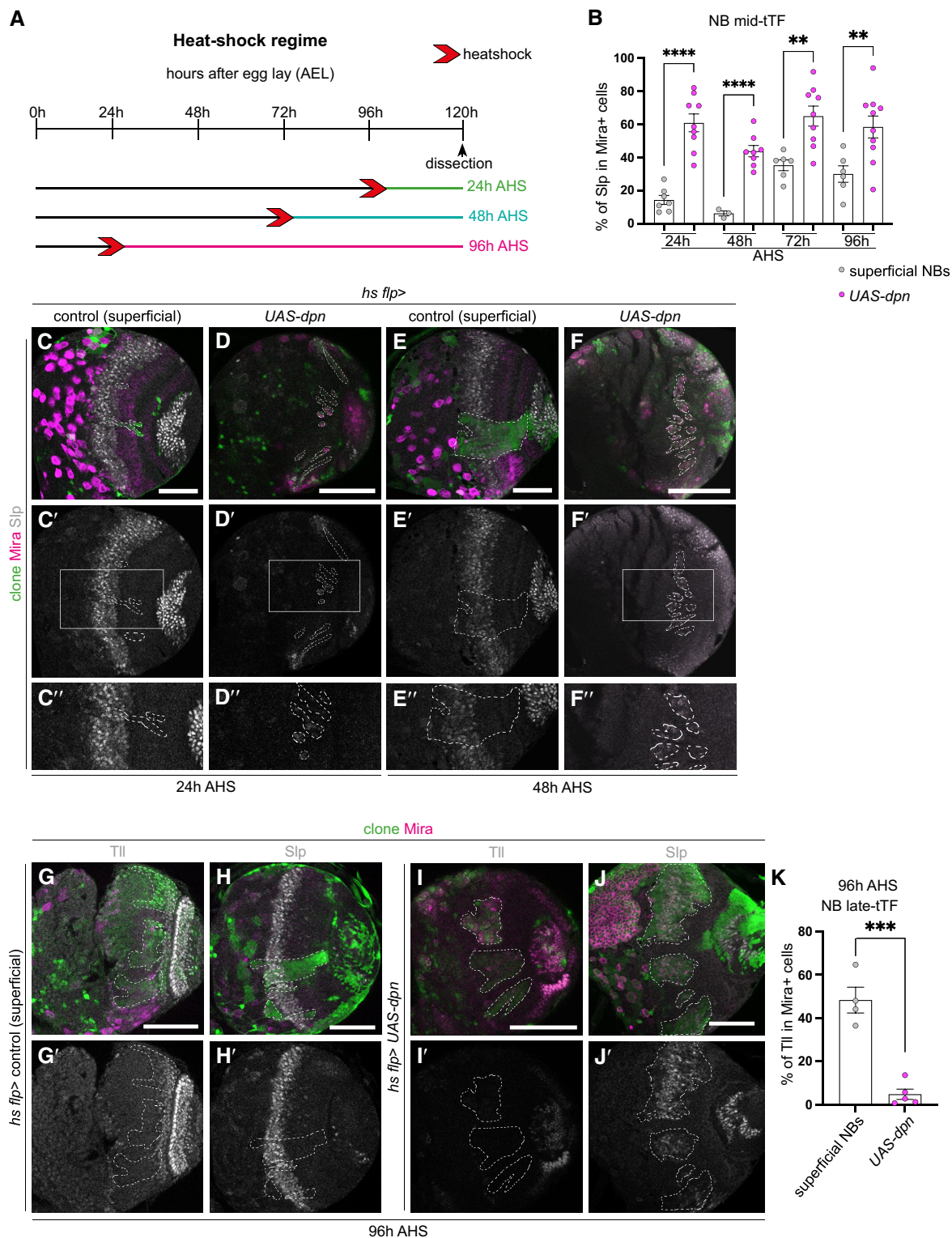


Figure 3.

Figure 3. Ectopic NBs generated via *dpn* overexpression immediately adopt a mid-temporal identity.

- A Schematic depicting the heat shock regimes used in (B–F') and (G–K'). Clones were induced via heat shock (red arrows) and dissected at 24 h (green), 48 h (turquoise), or 96 h (pink) after heat shock.
- B Quantification of % of Slp⁺ cells in Mira⁺ cells in control and *UAS-dpn* clones (expressed as the ratio between Slp⁺ volume and total Mira⁺ volume within a clone). 24 h (Control *n* = 7, *m* = 14.25 ± 2.696, *UAS-dpn* *n* = 9, *m* = 60.66 ± 5.384), 48 h (Control *n* = 3, *m* = 6.096 ± 1.509, *UAS-dpn* *n* = 8, *m* = 43.64 ± 3.398), 72 h (Control *n* = 6, *m* = 35.13 ± 3.242, *UAS-dpn* *n* = 9, *m* = 64.72 ± 6.045), 96 h (Control *n* = 6, *m* = 29.85 ± 4.951, *UAS-dpn* *n* = 10, *m* = 58.2 ± 6.603).
- C–F' Representative images of the deep medulla neuronal layer in the larval optic lobe, in which *UAS-dpn* or control are driven by *hs flp* (marked by GFP and outlined) and dissected and stained with the stem cell marker, Miranda (Mira, magenta), and Sloppy-paired (Slp, grey). At 24 and 48 h after clone induction, Mira⁺ NBs express mid tTF Slp compared to superficial NB control, quantified in (B). (C', D', E', F') are the magnified images of the square region outlined in (C', D', E', F'), respectively.
- G–J' At 96 h after clone induction, Mira⁺ NBs express mid tTF Slp and do not express late tTF Tll, compared to control, quantified in (B and K).
- K Quantification of % of Tll⁺ cells in Mira⁺ cells in control and *UAS-dpn* clones (expressed as the ratio between Tll⁺ volume and total Mira⁺ volume within a clone). Control *n* = 4, *m* = 48.34 ± 5.956, *UAS-dpn* *n* = 5, *m* = 4.805 ± 2.375.
- Data information: Data are represented as mean ± SEM. *P*-values were obtained performing unpaired *t*-test, and Welch's correction was applied in case of unequal variances. *****P* < 0.0001, ****P* < 0.001, ***P* < 0.005, **P* < 0.05. Scale bars: 50 μm.

mid-tTF Slp (Fig 8F and G). Consequently, this also resulted in an increase in the amount of Tll⁺ neurons (Fig 8D–D'') and a reduction in Toy⁺ progeny (Fig 8I–I').

We next asked whether dedifferentiation mediated by the down-regulation of Lola also stalled the temporal series. As previously reported, the expression of *lola*-RNAi caused neuron to NB dedifferentiation in the medulla (Fig 9A–E, Southall *et al.*, 2014; Zhu *et al.*, 2022). Furthermore, the dedifferentiated NBs expressed the mid-temporal series marker Slp (Fig 9A–F), which produced an excess of Toy⁺ neurons (Fig 9A–C''') and G), at the expense of Tll⁺ neurons and Repo⁺ glial cells (Fig 9H–J''', K and L). Overexpression of D, known to repress Slp, was able to promote the re-initiation of the temporal series, by reducing Slp expressing (Fig 9F), triggering the onset of Tll in the dedifferentiated NBs (Fig 9K), and the production of Tll⁺ neurons and Repo⁺ glial cells (Fig 9L), however, not Toy⁺ neurons (Fig 9G). Together, our data suggest that D overexpression can promote temporal progression stalled via Dpn overexpression, Notch activation or Lola knockdown.

Finally, we investigated whether *nerfin-1* loss-of-function clones also exhibited stalled temporal identity. In contrast to Dpn, N overexpression and Lola knockdown, *nerfin-1* mutant clones exhibited normal progression through the Hth → Ey → Slp → D temporal transcription factor widows (Fig EV5A–G' and J). However, as previously reported (Zhu *et al.*, 2022), the loss of *nerfin-1* caused stalling of the temporal series at Tll (Fig EV5A–G' and J), preventing the Tll⁺ neurogenesis to gliogenesis transition, as indicated by a deficit of Repo⁺ glial cells at 96-h AEL (Fig EV5H–I' and K).

Discussion

In this study, our data argue that upon NB dedifferentiation in the OL, the proliferative potential of NBs and their ability to produce the correct neuronal subtypes is determined by cell cycle progression and correct expression of the temporal transcription factors (tTFs). When ectopic NBs are induced by Dpn overexpression, they

Figure 4. NBs generated via Dpn overexpression delays the timing of their terminal differentiation and generates Toy⁺ progeny at the expense of Tll⁺ neurons and Repo⁺ glial cells.

- A Schematic depicting the timeline of experiments performed in (B–L'). Larval brains are dissected at 96 h, pupal brains are dissected at 126 h (6 h APF), 130 h (10 h APF), 136 h (16 h APF), and 144 h AEL (24 h APF). Heat shock regime for (Q–T'). Clones were induced by heat shock (red) at 48-h AEL and dissected 72 h (blue) after heat shock.
- B–M (B–I, K–L') Representative images of the superficial medulla neuroblast (NB) layer or deep medulla neuronal layer in the larval or pupal optic lobe, in which *UAS-dpn* or control (*UAS-luciferase*) are driven by *eyR16F10-GAL4*, or *ok107-GAL4* (outlined) and stained with the stem cell marker, Miranda (Mira, magenta), and mid-temporal progeny marker, Toy-GFP (grey). (B–E) Mira⁺ NBs are recovered in superficial sections of control under *eyR16F10-GAL4* expression at 6 h APF and 10 h APF but not from 16 h APF onwards, quantified in (J). (F–I) Mira⁺ NBs are recovered in deep sections of *UAS-dpn* driven by *eyR16F10-GAL4* at 6 h APF, 10 h APF, and 16 h APF but not at 24 h APF, quantified in (J). Arrow in (H) points to the NBs. (J) Quantification of % Mira⁺ cells within *eyR16F10-GAL4* expression domain in control and *UAS-dpn* (calculated as the ratio of Mira⁺ cell volume as a percentage of total *eyR16F10-GAL4* domain volume). Six hours APF (Control, *n* = 3, *m* = 14.82 ± 3.521, *UAS-dpn*, *n* = 6, *m* = 18.13 ± 1.46), 10 h APF (Control *n* = 4, *m* = 11.65 ± 1.605, *UAS-dpn* *n* = 5, *m* = 19.11 ± 4.609), 16 h APF (Control *n* = 4, *m* = 0.8897 ± 0.239, *UAS-dpn* *n* = 7, *m* = 16.64 ± 3.065), 24 h APF (Control *n* = 4, *m* = 1.174, ±0.7226, *UAS-dpn* *n* = 6, *m* = 0.8518 ± 0.4849). (K–L') More Toy⁺ progeny (grey) are present within the *ok107-GAL4* domain (green, outlined) in *UAS-dpn* compared to control. Quantified in (M). (M) Quantification of % Toy⁺ progeny within *ok107-GAL4* expression domain in control and *UAS-dpn* (calculated as the ratio of Toy⁺ cell volume as a percentage of total *ok107-GAL4* domain volume). Control *n* = 6, *m* = 11.03 ± 1.169, *UAS-dpn* *n* = 9, *m* = 22.78 ± 4.174.
- N Schematic representation of temporal series in NBs and their progeny. NBs express temporal transcription factors (tTFs; Hth, Ey, Slp, D, Tll) as they age. Slp⁺ NBs create Toy⁺ progeny; Tll⁺ NBs create Tll⁺ progeny; Gcm⁺ NBs create Repo⁺ progeny.
- O–R' Representative images of the deep medulla neuronal layer in the larval optic lobe, in which heat shock-induced *UAS-dpn* or control (*UAS-luciferase*) clones are stained with the stem cell marker, Mira (magenta), late neuronal marker Tll (grey) or glial marker Repo (grey). Arrow points towards the small band of Tll⁺ neurons in control clones. (O–P') At 72 h after clone induction, there is less Tll expression within *UAS-dpn* clones than control clone, quantified in (S). (Q–R') At 72 h after clone induction, there is less Repo expression within *UAS-dpn* clones than control clones, quantified in (T).
- S, T Quantification of % Tll or Repo⁺ cells within control and *UAS-dpn* clones (calculated as the ratio of Tll⁺ or Repo⁺ cell volume as a percentage of total clone volume). Tll (Control *n* = 6, *m* = 12.26 ± 3.449, *UAS-dpn* *n* = 5, *m* = 1.881 ± 0.9293), Repo (Control *n* = 7, *m* = 10.94 ± 2.203, *UAS-dpn* *n* = 4, *m* = 1.89 ± 0.2754).
- Data information: Data are represented as mean ± SEM. *P*-values were obtained by unpaired *t*-test, and Welch's correction was applied in case of unequal variances. ***P* < 0.005, **P* < 0.05. Scale bars: 50 μm.

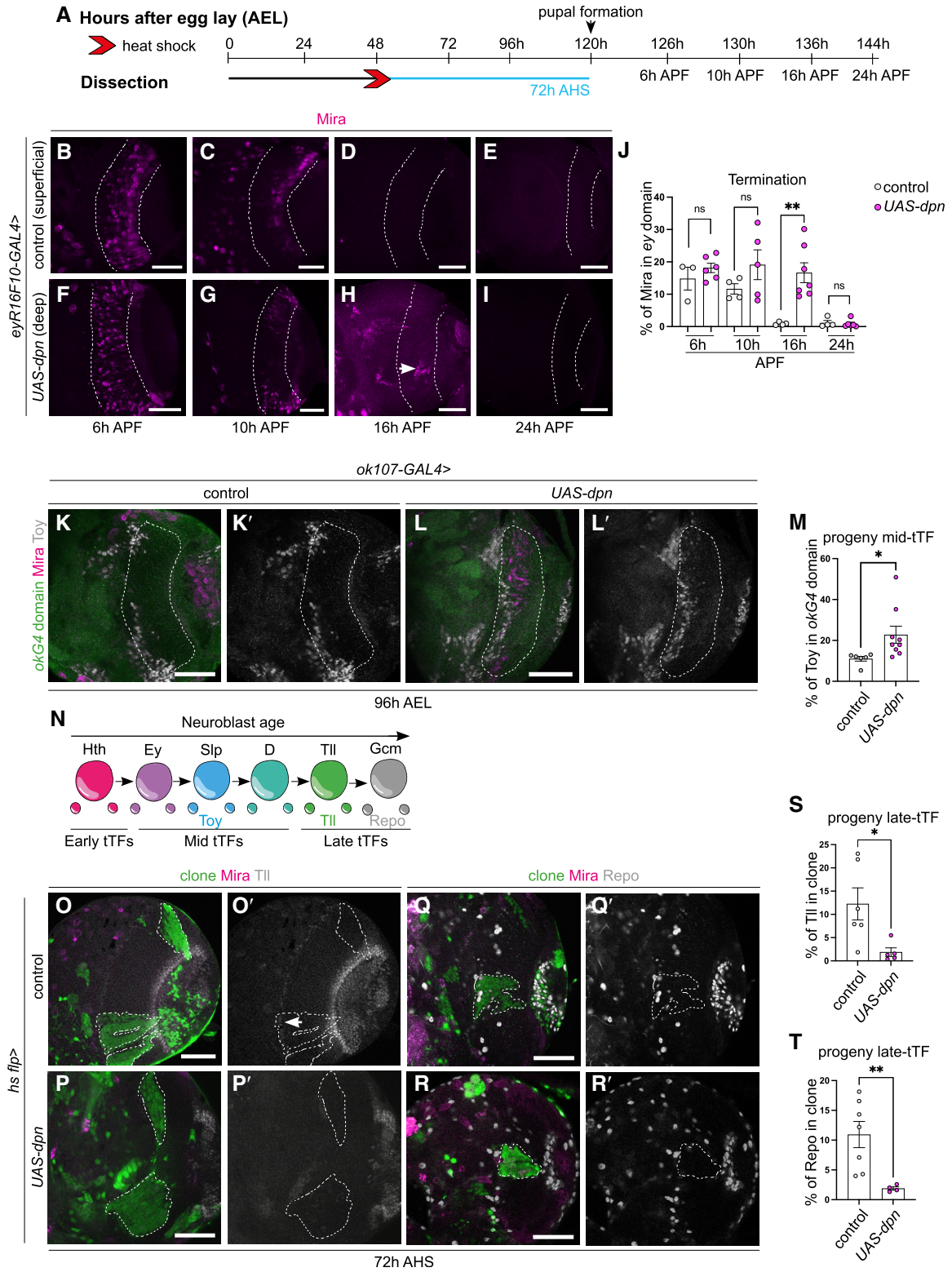


Figure 4.

adopt a mid-temporal identity, leading to significantly increased numbers of mid-temporal identity progeny. They also have delays in cell cycle progression and terminal cell cycle exit. Retriggering

the temporal series via D overexpression or promoting the cell cycle was sufficient to reinstate neuronal diversity and timely NB termination.

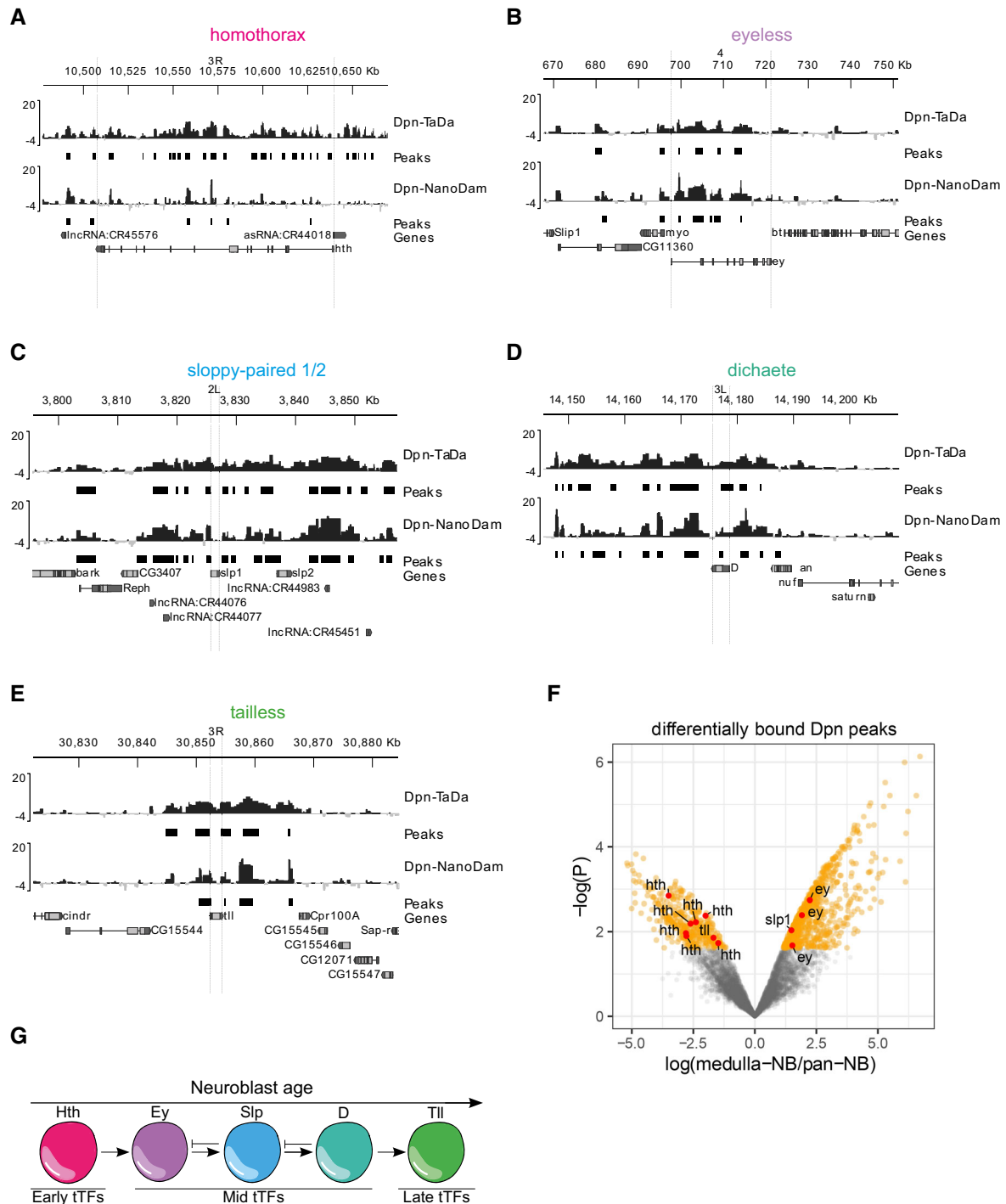


Figure 5. Dpn binds to tTFs with preference to mid-tTFs.

A–E Mean Targeted DamID Dpn (pan-neuroblast, NB) and Dpn-NanoDam (medulla specific) binding profiles ($\log_2(\text{Dam-fusion}/\text{Dam})$) are shown for the optic lobe temporal TFs (A) *homothorax* (B) *eyeless* (C) *sloppy-paired 1/2* (D) *dichaete* and (E) *tailless*. Peaks with $\text{FDR} < 0.01$ are shown.

F Volcano plot of differentially-bound Dpn peaks in the medulla show that Dpn preferentially bind preferentially to mid-tTFs *Slp1/2* and *Ey*, but not to early or late tTFs *Hth* or *Tll*.

G Schematic representation of temporal series in NBs. NBs express temporal transcription factors (tTFs; *Hth*, *Ey*, *Slp*, *D*, *Tll*) as they age.

Although ectopic NBs formed through Dpn overexpression were locked into a mid-temporal fate, we found that temporal transitions in dedifferentiated NBs obey the feed forward activation and

feedback repression that occurs in wild-type medulla NBs (Fig EV3C–D’). The mid-tTFs sit within a mutually exclusive regulatory network in which only one tTF can be active at any stage (Li

et al, 2013; Zhu et al, 2022), and consistent with this, we observed D to be expressed in a complementary pattern to that of Slp in ectopic NBs. The preference of Dpn binding at the mid-tTFs in medulla NBs, together with the enrichment of the mid-tTF fates,

suggests a model in which Dpn overexpression activates the mid-tTF network in ectopic NBs. Consistent with this, we observed enriched binding of Dpn at mid-tTF loci in wild-type medulla NBs, and reduced Dpn binding at early- and late-tTF loci. Our data

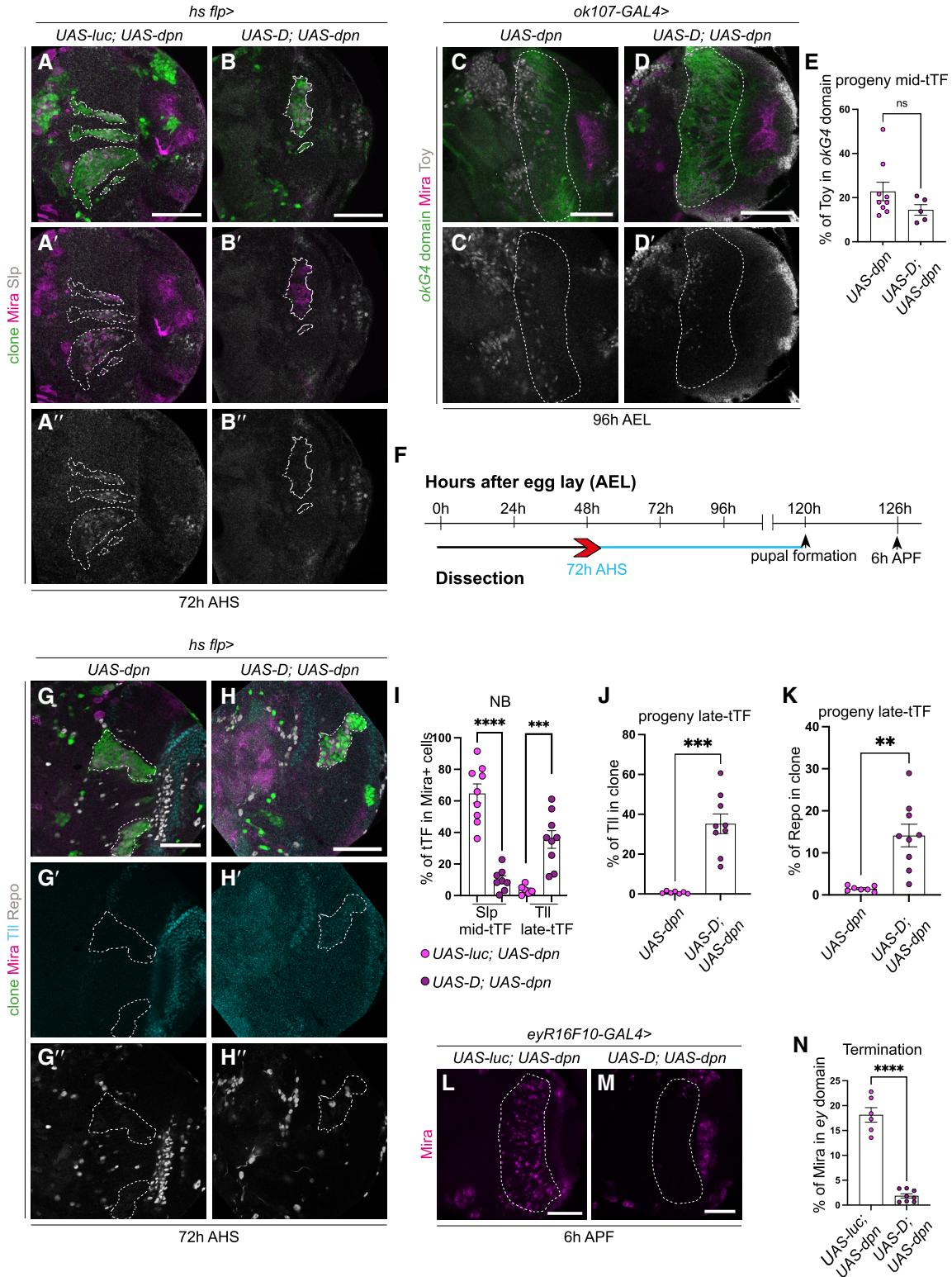


Figure 6.

Figure 6. Dichaete triggers the re-initiation of the temporal series.

A–H" (A–B" and G–H") Representative images of deep medulla neuronal layer in the larval optic lobe, in which *UAS-luc*; *UAS-dpn* and *UAS-D*; *UAS-dpn* are expressed in clones by *hs flp*, and stained with the stem cell marker, Miranda (Mira, magenta), and/or Slp, Tll or Repo (grey). (A–B") At 72 h after clone induction, *Mira*⁺ neuroblasts (NBs) within *UAS-luc*; *UAS-dpn* clones express Slp; *Mira*⁺ NBs within *UAS-D*; *UAS-dpn* clones do not express Slp, quantified in (I). (C–D") Representative images of deep medulla neuronal layer in the larval optic lobe, in which *UAS-dpn* and *UAS-D*; *UAS-dpn* are expressed in the *ok107-GAL4* expression domain, and stained with the stem cell marker, Mira (magenta), and mid-temporal progeny marker, Toy-GFP (grey). Fewer *Toy*⁺ cells were recovered within the *ok107-GAL4* domain (outlined) in *UAS-D*; *UAS-dpn* compared to *UAS-dpn*, quantified in (E). (E) Quantification of % *Toy*⁺ cells within *ok107-GAL4* expression domain in *UAS-dpn* and *UAS-D*; *UAS-dpn* (calculated as the ratio of *Toy*⁺ cell volume as a percentage of total *ok107-GAL4* domain volume). *UAS-dpn* *n* = 9, *m* = 22.78 ± 4.174, *UAS-D*; *UAS-dpn* *n* = 5, *m* = 14.42 ± 2.394. (F) Timeline depicting the age of ectopic neuroblasts. Pupal formation occurs at 120 h AEL. Pupae are dissected at 126-h AEL (6-h APF). Heat shock regime for (A–B") and (G–H"). Clones were induced by heat shock (red) at 48 h AEL and dissected at 72-h (blue) after heat shock. (G–H") At 72 h after clone induction, more *Tll*⁺ and *Repo*⁺ cells were recovered within *UAS-D*; *UAS-dpn* clones compared to *UAS-dpn* clones, quantified in (I–K).

I Quantification of % of *Slp*⁺ or *Tll*⁺ cells in *Mira*⁺ cells *UAS-luc*; *UAS-dpn* clones compared to *UAS-D*; *UAS-dpn* clones (expressed as the ratio between *tTF*⁺ volume and total *Mira*⁺ volume within a clone). *Slp* (*UAS-luc*; *UAS-dpn* *n* = 9, *m* = 64.72 ± 6.045, *UAS-D*; *UAS-dpn* *n* = 8, *m* = 9.99 ± 2.463), *Tll* (*UAS-luc*; *UAS-dpn* *n* = 6, *m* = 3.584 ± 1.187, *UAS-D*; *UAS-dpn* *n* = 9, *m* = 35.53 ± 5.596).

J, K Quantification of % *Tll*⁺ or *Repo*⁺ cells within *UAS-dpn* clones compared with *UAS-D*; *UAS-dpn* clones (calculated as the ratio of *Tll*⁺ or *Repo*⁺ cell volume as a percentage of total clone volume). *Tll* (*UAS-dpn* *n* = 7, *m* = 0.7198 ± 0.2389, *UAS-D*; *UAS-dpn* *n* = 9, *m* = 35.22 ± 4.917), *Repo* (*UAS-dpn* *n* = 7, *m* = 1.488 ± 0.2368, *UAS-D*; *UAS-dpn* *n* = 9, *m* = 14.13 ± 2.672).

L, M *Mira*⁺ NBs are present in deep sections of *UAS-dpn* driven by *eyR16F10-GAL4* at 126 h but are absent in *UAS-D*; *UAS-dpn*, quantified in (N).

N Quantification of % *Mira* cells within *eyR16F10-GAL4* expression domain in *UAS-dpn* and *UAS-D*; *UAS-dpn* (calculated as the ratio of *Mira*⁺ cell volume as a percentage of total *eyR16F10-GAL4* domain volume). *UAS-dpn* *n* = 6, *m* = 18.13 ± 1.46, *UAS-D*; *UAS-dpn* *n* = 8, *m* = 1.859 ± 0.4215.

Data information: Data are represented as mean ± SEM. *P*-values were obtained via unpaired *t*-test, and Welch's correction was applied in cases of unequal variances. *****P* < 0.0001, ****P* < 0.001, ***P* < 0.005. Scale bars: 50 μm.

suggest that Dpn promotes the expression of mid-tTFs such as *Ey* and *Slp* (Fig 9M). Although Dpn has been historically classed as a transcriptional repressor, a previous study profiling Dpn binding in larval NB hyperplasia via ChIP-seq reported that half of the directly regulated targets of Dpn were upregulated in tumours, and half were downregulated, consistent with a dual activator/repressor role for this protein (Magadi *et al*, 2020).

The delay in temporal progression appears to be a general feature of dedifferentiation in the OL, as a delay in dedifferentiation was observed upon Dpn or Notch activation, as well as the downregulation of *Lola* and *Nerfin-1*. The OL is an area of the brain where the differentiated state of the neurons appears to be less stable (Xu *et al*, 2017). However, we do not yet know whether dedifferentiation-mediated tumours arising from other regions of the CNS would also exhibit delayed temporal progression, as different

sets of temporal factors are used in the ventral nerve cord and Type II lineages (Maurange *et al*, 2008; Ren *et al*, 2017). It would be interesting to explore whether N or tumour suppressors such as Brain Tumour (Brat) similarly regulate the mid-tTF genes, as it has previously been shown that Brat regulates both Dpn and Notch (Reichardt *et al*, 2018). However, it could be that N acts partially through Dpn, as Dpn has been shown to be a target of N in NBs (San-Juán *et al*, 2012).

Our data support the possible links between cell cycle progression and the expression of temporal regulators controlling NB proliferation and cellular diversity. In the embryonic NBs, temporal transition can progress despite of experimentally induced cell cycle arrest (Grosskortenhous *et al*, 2005). Whereas in Type I larval NBs, it was shown that G1/S-cell cycle delay resulted in stalled temporal patterning and reduced neuronal

Figure 7. Temporal progression of dedifferentiated NBs is regulated by the cell cycle.

A–C" Representative images of the deep medulla neuronal layer in the larval optic lobe, in which control (*UAS-luc*) and *UAS-dpn* and *UAS-D*; *UAS-dpn* are expressed in *hs flp* clones (72 h after clone induction). Miranda (Mira, magenta) and EdU (grey). Despite increased number of *Mira*⁺ cells in *UAS-dpn* compared to control, each neuroblast (NB) underwent slower cell cycle progression, as indicated by EdU⁺ incorporation. Quantified in (E). This slow cell cycle speed was not rescued in *UAS-D*; *UAS-dpn* clones. Quantified with *UAS-luc*; *UAS-dpn* in (F).

D Heat shock regime for (A–C"). Clones were induced by heat shock (red) at 48-h AEL and dissected 72-h (blue) after heat shock.

E Quantification of % of EdU-positive cells in control (*UAS-luc*) and *UAS-dpn* clones (expressed as the amount of EdU⁺ cells per *Mira*⁺ volume within the clone). Control *n* = 6, *m* = 4.96 ± 0.5433, *UAS-dpn* *n* = 10, *m* = 0.5927 ± 0.08484.

F Quantification of % of EdU-positive cells in *UAS-luc*; *UAS-dpn* and *UAS-D*; *UAS-dpn* clones (expressed as the amount of EdU⁺ cells per *Mira*⁺ volume within the clone). *UAS-luc*; *UAS-dpn* *n* = 9, *m* = 0.7807 ± 0.1311, *UAS-D*; *UAS-dpn* *n* = 10, *m* = 0.4866 ± 0.3579.

G–H" Representative images of the deep medulla neuronal layer in the larval optic lobe, where *UAS-E2f1*; *UAS-CycE*; *UAS-dpn* or *UAS-dpn* are expressed in the *ok107-GAL4* domain (outlined), and stained with the stem cell marker, Mira (magenta), mid-tTF, Slp (grey) and late progeny marker, Repo (Cyan). Quantified in (I–K). *UAS-dpn* NBs express Slp and do not create *Repo*⁺ progeny, whereas *UAS-E2f1*; *UAS-CycE*; *UAS-dpn* NBs do not express Slp and create *Repo*⁺ progeny.

I Quantification of % *Mira*⁺ cells within *ok107-GAL4* expression domain in *UAS-dpn* control and *UAS-E2f1*; *UAS-CycE*; *UAS-dpn* (calculated as the ratio of *Mira*⁺ cell volume as a percentage of total *ok107-GAL4* volume). *UAS-dpn* control *n* = 8, *m* = 27.99 ± 5.288, *UAS-E2f1*; *UAS-CycE*; *UAS-dpn* *n* = 7, *m* = 42.37 ± 3.999.

J Quantification of % *Slp*⁺ cells in *Mira*-positive cells within the *ok107-GAL4* expression domain in *UAS-dpn*; *UAS-luc* and *UAS-E2f1*; *UAS-CycE*; *UAS-dpn* (calculated as the ratio of *Slp*⁺ cellular volume as a percentage of total *Mira*⁺ volume within *ok107-GAL4* domain). *UAS-dpn* control *n* = 7, *m* = 50.76 ± 2.582, *UAS-E2f1*; *UAS-CycE*; *UAS-dpn* *n* = 8, *m* = 2.907 ± 0.5755.

K Quantification of % *Repo*⁺ progeny in within the *ok107-GAL4* expression domain in *UAS-dpn*; *UAS-luc* and *UAS-E2f1*; *UAS-CycE*; *UAS-dpn* (calculated as the ratio of *Repo*⁺ cellular volume within *ok107-GAL4* domain). *UAS-dpn* control *n* = 10, *m* = 2.567 ± 0.491, *UAS-E2f1*; *UAS-CycE*; *UAS-dpn* *n* = 7, *m* = 6.977 ± 0.8049.

L Schematic representation of the cell cycle. *Cdk4/CycD* and *E2f/CycE* play roles in G1/S phase transition. *E2f/CycE* play a role in G1/S and G2/M phase transitions.

Data information: Data are represented as mean ± SEM. *P*-values were obtained performing unpaired *t*-test, and Welch's correction was applied in case of unequal variances. *****P* < 0.0001, ****P* < 0.001, ***P* < 0.005, **P* < 0.05. Scale bars: 50 μm.

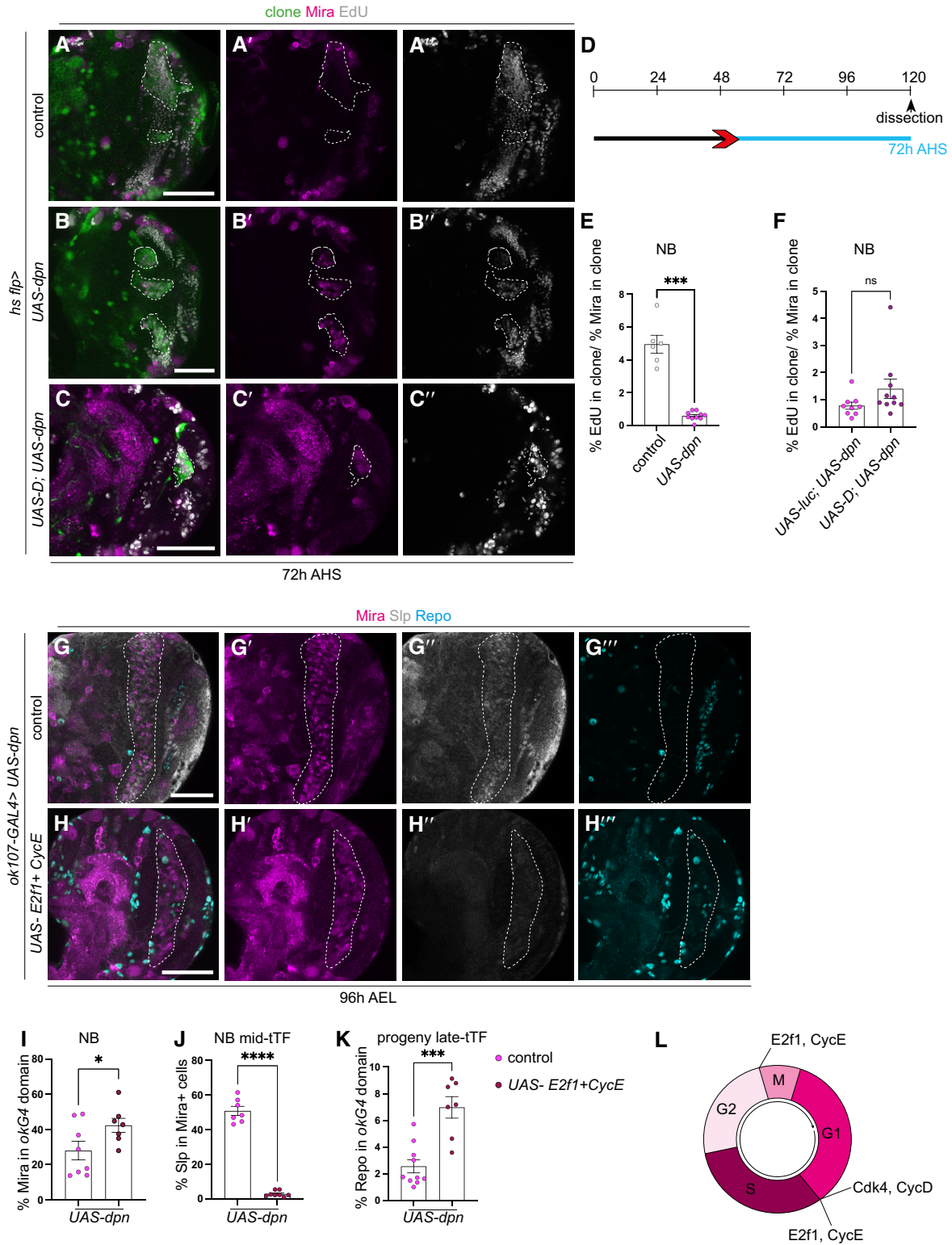


Figure 7.

diversity (van den Amelee & Brand, 2019). In dedifferentiated OL NBs, it appears that the temporal series also lies downstream of the cell cycle. However, in this context, we show that the cell cycle can direct and regulate the progression of the

temporal series and is responsible for restoring neuronal diversity caused by temporal series delay. However, re-initiation of the temporal series was not sufficient to rescue cycle progression.

Perturbation of different neuronal factors can impact different points of the neurogenesis temporal series. It is so far unclear why *nerfin-1* mutant clones differ from the other dedifferentiation factors,

where they are stalled at the Tll⁺ window rather than Slp⁺ window. Future studies using ATAC-seq to examine the chromatin accessibility of the temporal transcription factors for each of these dedifferentiation

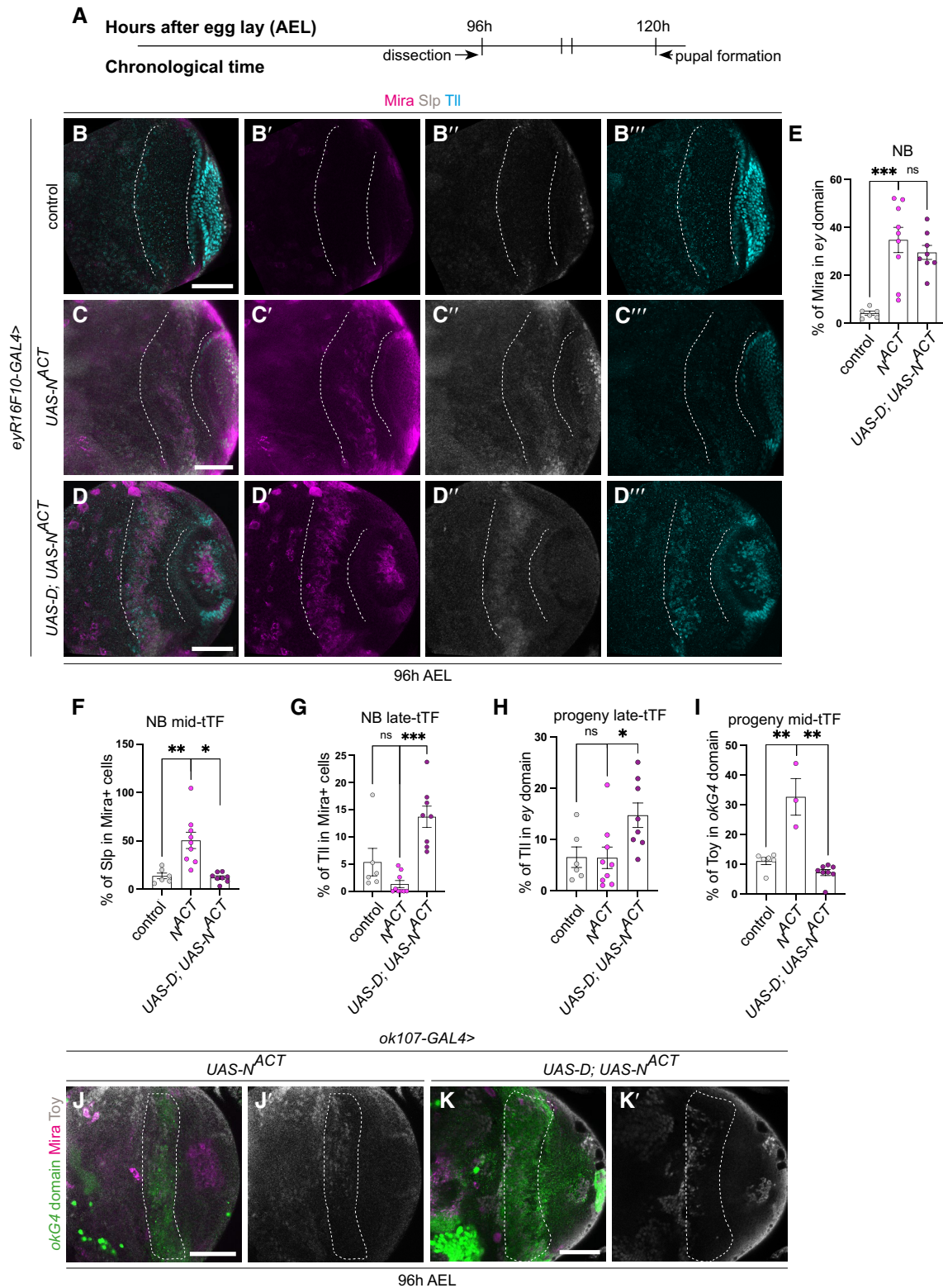


Figure 8.

Figure 8. Dichaete re-initiates the temporal series in dedifferentiated NBs caused by Notch activation.

- A Timeline depicting age of ectopic neuroblasts (NBs). Larvae are dissected at 96 h AEL.
- B–D^{'''} Representative images of the deep medulla neuronal layer in the larval optic lobe, in which control (*UAS-luc*), *UAS-N^{ACT}*, and *UAS-D; UAS-N^{ACT}* are driven by *eyR16F10-GAL4* (outlined). Miranda (Mira, magenta), Sloppy paired (Slp, grey), Tailless (Tll, cyan). *UAS-N^{ACT}* NBs express Slp and not Tll. *UAS-D; UAS-N^{ACT}* NBs express Slp and Tll, quantified in (E–H).
- E Quantification of % Mira-positive cells within *eyR16F10-GAL4* expression domain in control, *UAS-N^{ACT}*, and *UAS-D; UAS-N^{ACT}* (calculated as the ratio of Mira⁺ cell volume as a percentage of total volume of *eyR16F10-GAL4* domain). Control *n* = 6, *m* = 4.077, ±2.103, *UAS-N^{ACT}* *n* = 9, *m* = 34.71, ±5.271, *UAS-D; UAS-N^{ACT}* *n* = 8, *m* = 29.5, ±2.931.
- F, G Quantification of % Slp⁺ or Tll⁺ cells in Mira-positive cells within the *eyR16F10-GAL4* expression domain in control, *UAS-N^{ACT}*, and *UAS-D; UAS-N^{ACT}* (calculated as % of Slp⁺ or Tll⁺ cellular volume that are also Mira⁺ within *eyR16F10-GAL4* domain). Slp (Control *n* = 6, *m* = 13.62 ± 2.974, *UAS-N^{ACT}* *n* = 9, *m* = 13.62 ± 2.974, *UAS-D; UAS-N^{ACT}* *n* = 8, *m* = 11.98 ± 1.741), Tll (Control *n* = 6, *m* = 5.363 ± 2.531, *UAS-N^{ACT}* *n* = 9, *m* = 1.316 ± 0.643, *UAS-D; UAS-N^{ACT}* *n* = 8, *m* = 13.71 ± 1.955).
- H Quantification of % Tll⁺ cells within *eyR16F10-GAL4* expression domain in control, *UAS-N^{ACT}*, and *UAS-D; UAS-N^{ACT}* (calculated as the ratio of Tll⁺ cellular volume as a percentage of total volume of *eyR16F10-GAL4* domain). Control *n* = 6, *m* = 6.554 ± 2.018, *UAS-N^{ACT}* *n* = 9, *m* = 6.449 ± 2.099, *UAS-D; UAS-N^{ACT}* *n* = 8, *m* = 14.77 ± 2.404.
- I Quantification of % Toy⁺ cells within *ok107-GAL4* expression domain in control (*UAS-luc*), *UAS-N^{ACT}* and *UAS-N^{ACT}; UAS-dpn* (calculated as the ratio of Toy⁺ cell volume as a percentage of total *ok107-GAL4* domain volume). The column for Control uses the same data points as in Fig 3K. Control *n* = 6, *m* = 11.03 ± 1.169, *UAS-N^{ACT}* *n* = 3, *m* = 32.65 ± 6.176, *UAS-N^{ACT}; UAS-dpn* *n* = 8, *m* = 7.178 ± 1.023).
- J–K['] Representative images of the deep medulla neuronal layer in the larval optic lobe, in which *UAS-N^{ACT}* and *UAS-N^{ACT}; UAS-dpn* are driven by *ok107-GAL4* (marked by GFP and outlined) and stained with the stem cell marker, Mira (magenta), and mid-temporal progeny marker, Toy-GFP (grey). Fewer cells express Toy⁺ in *UAS-N^{ACT}; UAS-dpn* compared to *UAS-N^{ACT}*, quantified in (I).
- Data information: Data are represented as mean ± SEM. *P*-values were obtained performing unpaired *t*-test, and Welch's correction was applied in case of unequal variances. *****P* < 0.0001, ****P* < 0.001, ***P* < 0.005. Scale bars: 50 μm.

factors may shed light on the specificity. However, our work together with previous work using another dedifferentiation tumour model (*pros* loss of function) shows that specification of the correct temporal cascade is instrumental to tumour malignancy and is a key mechanism underlying tumourigenesis (Narbonne-Reveau *et al*, 2016; Genovese *et al*, 2019; Maurange, 2020; Gaultier *et al*, 2022).

Recent studies suggest that a bidirectional conversion between tumour-initiating stem cells and differentiated cells exist, where non-cancer stem cells can dedifferentiate and acquire stem cell-like properties under genetic and environmental stress (Friedmann-Morvinski & Verma, 2014). Dedifferentiation of mature cells to induce their proliferation and re-differentiation has also been shown

Figure 9. Dichaete re-initiates the temporal series in dedifferentiated NBs caused by the loss of Lola.

- A–C^{'''} Representative images of the deep medulla neuronal layer in the larval optic lobe, in which control (*UAS-lacZ*), *lola-Ri*, and *UAS-D; lola-Ri* are driven by *eyR16F10-GAL4* (outlined). Miranda (Mira, magenta), Sloppy-paired (Slp, grey), Twin of eyeless (Toy, cyan). *lola-Ri* induces ectopic Mira⁺ neuroblasts (NBs) in the deep medulla layers, compared to control, quantified in (E). Dedifferentiated *lola-Ri* NBs express excess Slp, fewer Tll, and slightly more Toy⁺ neurons compared to control. *UAS-D; lola-Ri* NBs express less Slp and similar amount of Toy in *eyR16F10-GAL4* domain compared to *lola-Ri* alone, quantified in (F, G).
- D Timeline depicting the age of ectopic neuroblasts (NBs). Larvae are dissected at 96 h AEL.
- E Quantification of % Mira-positive cells within *eyR16F10-GAL4* expression domain in control, *lola-Ri*, and *UAS-D; lola-Ri* (calculated as the ratio of Mira⁺ cell volume as a percentage of total volume of *eyR16F10-GAL4* domain). Control *n* = 8, *m* = 2.717, ±0.9933, *lola-Ri* *n* = 11, *m* = 36.95, ±5.447, *UAS-D; lola-Ri* *n* = 17, *m* = 25.57, ±3.303.
- F Quantification of % Slp⁺ cells in Mira-positive cells within the *eyR16F10-GAL4* expression domain in control, *lola-Ri*, and *UAS-D; lola-Ri* (calculated as % of Slp⁺ cellular volume that are also Mira⁺ within *eyR16F10-GAL4* domain). Control *n* = 8, *m* = 22.80 ± 4.065, *lola-Ri* *n* = 7, *m* = 57.68 ± 7.234, *UAS-D; lola-Ri* *n* = 8, *m* = 6.482 ± 0.8840.
- G Quantification of % Toy⁺ cells within *eyR16F10-GAL4* expression domain in control, *lola-Ri*, and *UAS-D; lola-Ri* (calculated as the ratio of Toy⁺ cellular volume as a percentage of total volume of *eyR16F10-GAL4* domain). Control *n* = 8, *m* = 25.14 ± 4.109, *lola-Ri* *n* = 7, *m* = 44.16 ± 8.518, *UAS-D; lola-Ri* *n* = 9, *m* = 40.53 ± 2.633.
- H–J^{'''} Representative images of the deep medulla neuronal layer in the larval optic lobe, in which control (*UAS-lacZ*), *lola-Ri*, and *UAS-D; lola-Ri* are driven by *eyR16F10-GAL4* (outlined). Miranda (Mira, magenta), Tailless (Tll, grey), Reversed polarity (Repo, cyan). *lola-Ri* NBs express less Tll compared to control. There are fewer Tll⁺ and Repo⁺ progeny in the *eyR16F10-GAL4* domain in *lola-Ri* compared to control. *UAS-D; lola-Ri* NBs express more Tll as well as more Tll⁺ and Repo⁺ progeny in *eyR16F10-GAL4* domain compared to *lola-Ri* alone, quantified in (K, L).
- K Quantification of % Tll⁺ cells in Mira-positive cells within the *eyR16F10-GAL4* expression domain in control, *lola-Ri*, and *UAS-D; lola-Ri* (calculated as % of Tll⁺ cellular volume that are also Mira⁺ within *eyR16F10-GAL4* domain). Control *n* = 8, *m* = 14.82 ± 2.400, *lola-Ri* *n* = 4, *m* = 0.2982 ± 0.1217, *UAS-D; lola-Ri* *n* = 8, *m* = 46.85 ± 10.46.
- L Quantification of % Tll⁺ and Repo cells within *eyR16F10-GAL4* expression domain in control, *lola-Ri*, and *UAS-D; lola-Ri* (calculated as the ratio of Tll⁺ and Repo⁺ cellular volume as a percentage of total volume of *eyR16F10-GAL4* domain). Tll (Control *n* = 8, *m* = 10.94 ± 2.629, *lola-Ri* *n* = 4, *m* = 0.1024 ± 0.05082, *UAS-D; lola-Ri* *n* = 8, *m* = 19.26 ± 3.264), Repo (Control *n* = 8, *m* = 28.95 ± 6.330, *lola-Ri* *n* = 4, *m* = 9.648 ± 3.228, *UAS-D; lola-Ri* *n* = 8, *m* = 29.00 ± 7.984).
- M Upon Dpn overexpression, ectopic NBs were induced. These ectopic NBs expressed the mid-temporal tTF, Slp, and did not express early tTFs or late tTFs. Consequently, an excess of progeny was produced from the Slp⁺ temporal window at the expense of the progeny produced from late tTF time windows. DamID analysis demonstrated that Dpn directly bind to Ey and Slp, but not to Hth or Tll. Therefore, Dpn may be directly responsible for the increased expression of mid-temporal identity TFs in dedifferentiated NBs at the expense of early or late temporal TFs.
- Data information: Data are represented as mean ± SEM. *P*-values were obtained performing unpaired *t*-test, and Welch's correction was applied in case of unequal variances. *****P* < 0.0001, ****P* < 0.001, ***P* < 0.005, **P* < 0.05. Scale bars: 50 μm.

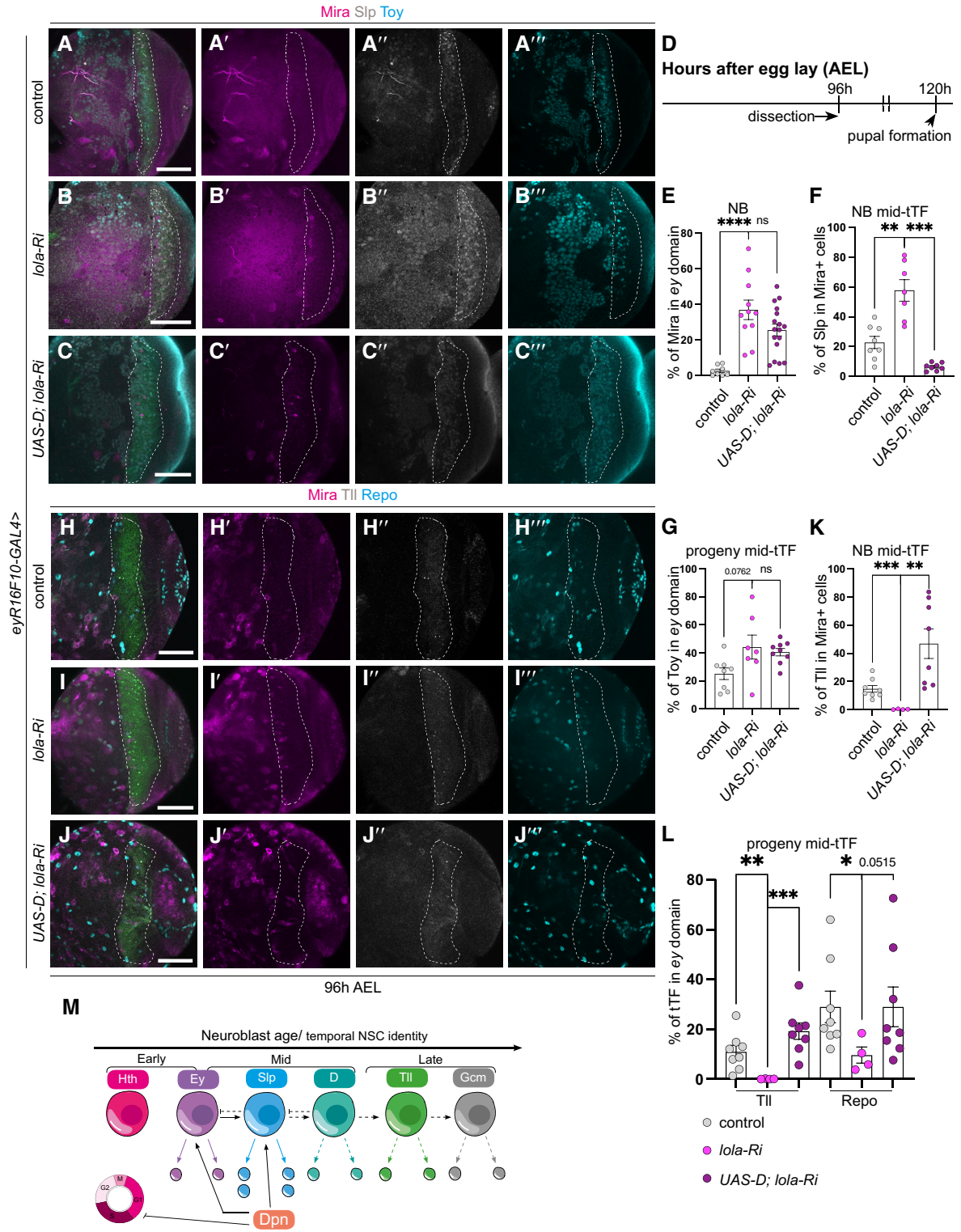


Figure 9.

to be a promising means of tissue repair and regeneration. Therefore, dedifferentiation may have either positive or negative consequences for tissue repair and tumorigenesis. Our work shows that

appropriate temporal and cell cycle progression controls are key to regulating the fine balance between tumorigenesis and controlled dedifferentiation.

Materials and Methods

Fly husbandry

Fly stocks were reared on standard *Drosophila* media at 25°C. For larval dissection, brains were dissected at wandering L3 stages. For pupal dissection, white pupae were selected and then allowed to age at 29°C, dissections were made at 6, 10, 16 or 24 h after pupal formation (APF).

GAL4 lines *GMR31H08-GAL4*, *ey^{OK107}-GAL4* and *eyR16F10-GAL4* were used to induce dedifferentiation. *GMR31H08-Gal4* (Jenett et al, 2012) is a neuronal-specific driver (Fig EV1E–F^{'''}), this line together with a GAL80-ts was used to demonstrate that mature neurons can undergo dedifferentiation (Fig EV1A–D). *ey^{OK107}-GAL4* (Morante et al, 2011) is expressed in both neurons and NBs during larval neurogenesis (Fig EV1I–J^{'''}), and *eyR16F10-GAL4* is expressed in both neurons and NBs (Fig EV1O–P^{'''}). *eyR16F10-GAL4* but not *ey^{OK107}-GAL4* was strongly expressed in the medulla neurons during pupal development (Fig EV1Q and R, and K and L); therefore, *eyR16F10-GAL4* was utilised in all the pupal analysis. *ey^{OK107}-GAL4* was used to make compound stocks with *Toy-GFP* and was restricted to larval analysis (Morante et al, 2011; Jenett et al, 2012). Knockdown or overexpression CNS clones were generated using the flpout system. *hsFLP; act5 > CD2 > Gal4, UAS-GFP/TM6b* (Vissers et al, 2018). Flpout clones were induced by heat shock at 16, 24, 48 h, 72 or 96 h after egg lay (AEL) for 6 min, shifted to 29°C and dissected at 120 h AEL. The fly strains used were as follows: *UAS-deadpan* (A. Baonza), (#1776, Bloomington), *UAS-Nerfin-1 RNAi* (VDR), *UAS-mCherry RNAi* (#35785, Bloomington), *Toy-GFP* (#83390, Bloomington), *UAS-N^{ACT}* (#52309, Bloomington), *UAS-Cdk4; UAS-CycD* (Helena Richardson), *UAS-E2f1; UAS-CycE* (Helena Richardson), *UAS-D* (#8861, Bloomington), *UAS-lola RNAi* (#35721, Bloomington). *Nerfin-1¹⁵⁷* mutant clones (Froldi et al, 2015) were generated using the MARCM system (w, tub-Gal4, UAS-nlsGFP::6xmyc::NLS, hs-flp; FRT2A, tubP-Gal80LL9/TM6B).

Immunostaining

Larval and pupal brains were dissected out in phosphate buffered saline (PBS), fixed for 20 min in 4% formaldehyde in PBS and rinsed in 0.2% PBST (PBS + 0.2% TritonX-100). For immunostaining, brains were incubated with primary antibodies overnight at 4°C, followed by an overnight secondary antibody incubation at 4°C. Samples were mounted in 80% glycerol in PBS for image acquisition. The primary antibodies used were mouse anti-Mira (1:50; gift of Alex Gould), rat anti-Mira (1:100, Abcam), rat anti-pH3 (1:500; Abcam), chick anti-GFP (1:2000; Abcam), rabbit anti-RFP (1:100, Abcam), mouse anti-Repo (1:50, DSHB), guineapig anti-Hth (1:100, Claude Desplan), mouse anti-Ey (1:50, DSHB), guineapig anti-Slp (1:500, Kuniaki Saito), rabbit anti-D (1:1,000, Steve Russell), guineapig anti-Tll (1:100, Kuniaki Saito), rabbit anti-Tll (1:100, Kuniaki Saito) and guineapig anti-Toy (1:50, Uwe Walldorf). Secondary donkey antibodies conjugated to Alexa 555 and Alexa 647, and goat antibody conjugated to Alexa 405, 488, 555 and 647 (Molecular Probes) were used at 1:500.

EdU pulse/chase

Control and *UAS-dpn* clones were induced 48 h AEL. 48 h after clone induction, larvae were fed with 100 mg/ml EdU for 3 h. They

were then transferred to standard medium for a 3h EdU-free chase. Larvae were dissected, fixed and processed for antibody staining, followed by EdU detection with Click-iT Plus EdU Cell Proliferation Kit for imaging, Alexa Fluor 647 dye (Invitrogen, #C10640) according to the manufacturer's instruction.

Imaging and image processing

Images were collected on a Leica SP5/Olympus FV3000 confocal microscope and processed using Fiji (<https://imagej.net/Fiji>). Z stacks of optic lobes were imaged, and single sections were shown as the representative image in the figures. All images represent the medulla deep section unless specifically stated.

GFP⁺, Mira⁺ NBs, Toy⁺ neurons, *ey^{OK107}-GAL4* expressing domain and TF volume were measured using fluorescence intensity from three-dimensional reconstructions of 2-μm spaced confocal Z-stacks with Volocity software (Improvision) or Imaris (Bitplane). The rate of dedifferentiation was represented as the volume of Mira⁺ cells as a percentage of clone volume. The percentage of TFs was calculated as the volume of TF⁺ cells as a percentage of clone volume or domain volume. The percentage of Toy⁺ neurons was calculated as the volume of Toy⁺ neurons as a percentage of *ey^{OK107}-GAL4* expressing domain volume. *eyR16F10-GAL4* domain was not labelled with a fluorescent marker, a Region of Interest (ROI) was manually selected in each of the slice across the Z sections, as guided by the outline of the overlaying superficial NBs.

Statistical analysis

At least three animals per genotype were used for all experiments. Volume of clones or regions of interest was estimated from three-dimensional reconstructions of 2-mm spaced confocal Z stacks with the Volocity software (Improvision).

In all graphs and histograms, error bars represent the standard error of the mean (SEM) and *P*-values are calculated by performing two-tailed, unpaired Student's *t*-test. The Welch's correction was applied in case of unequal variances.

Targeted DamID

FlyORF-TaDa-Dpn flies were created from the FlyORF-Dpn-3xHA line (FlyORF stock# F000086) with the FlyORF-TaDa system as previously described (Aughey et al, 2021). Targeted DamID for Dpn in 3rd instar larval neuroblasts was performed as previously described (Marshall & Brand, 2015; Marshall et al, 2016), crossing FlyORF-TaDa-Dpn flies with the neuroblast-specific wor-Gal4;tub-GAL80ts driver. NanoDam (Tang et al, 2022) for Dpn in 3rd instar larval medulla NBs was performed using *TaDaM-traNLS-vhhGFP* (preprint: Delandre et al, 2022) crossing *TaDaM-traNLS-vhhGFP, tub-GAL80ts; eyR16F10-GAL4* to either *Dpn-GFP* (BL# 65295) or the *w¹¹¹⁸* genetic background. In both cases, flies were allowed to lay on apple juice plates with yeast for 4 h at 25°C, before transferring plates to 18°C for 2 days. 100 larvae from each plate were transferred to food plates and grown at 18°C for a further 5 days, before shifting to the permissive temperature of 29°C. Two biological replicates were collected, of 30 dissected brains per replicate (Dpn TaDa) or 40 brains per replicate (Dpn NanoDam).

Samples were processed for DamID as previously described (Marshall et al, 2016). Briefly, genomic DNA was extracted, cut with

DpnI and cut fragments isolated. DamID adaptors were ligated to the isolated DNA, fragments were digested with DpnII, and amplified via PCR. Following PCR, samples were sonicated in a Bioruptor Plus (Diagenode) to reduce the average DNA fragment size to 300 bp, and DamID adaptors were removed via overnight AlwI digestion. The resulting DNA was purified via magnetic bead cleanup and 500 ng of DNA was end-repaired, A-tailed, ligated to NGS adaptors and amplified via six PCR cycles. The final libraries, multiplexed to yield ~20 million mappable fragments per sample, were sequenced as paired-end reads (MGI platform, BGI).

NGS reads in FASTQ format were aligned using `damidseq_pipeline` (Marshall & Brand, 2015) using default options, and replicates were averaged to give the final binding profile. Significantly enriched peaks were called for each replicate using `find_peaks` (Marshall *et al*, 2016) with parameters `--min-quant = 0.8` and `--unified_peaks = min` with otherwise default options; peaks were considered significant at $FDR < 0.01$. Peaks for all replicates and conditions were combined using the `GenomicRanges` R package, the per-replicate binding occupancy across each region determined, and differentially bound peaks were called using `NOISeq` (Tarazona *et al*, 2015) at $q = 0.85$. Peaks were associated with genes within ± 1 kb of a peak. Datasets were visualised using `pyGenomeTracks` (Cubenas-Potts *et al*, 2017).

Data availability

NGS data have been deposited in the NCBI Gene Expression Omnibus (GEO) and are available under accession number [GSE225409](https://www.ncbi.nlm.nih.gov/geo/query/acc.cgi?acc=GSE225409).

Expanded View for this article is available [online](#).

Acknowledgements

We are grateful to C. Desplan, H. Richardson, S. Russell, X Li, U. Walldorf, K. Saito, for generous sharing of antibodies and fly stocks. LYC is funded by an Australian Research Council (ARC) Future Fellowship (FT180100255), LYC's laboratory is supported by funding from the National Health and Medical Research Council of Australia (NHMRC 1182847), Australian Research Council (190101743) and the Peter MacCallum Cancer Foundation. KFH was supported by an NHMRC Investigator grant (APP1194467) and Australian Research Council (190101743). Confocal Microscopy was performed at the Centre for Advanced Histology & Microscopy (CAHM) at the Peter MacCallum Cancer Centre and the Biological Optical Microscopy Platform at the University of Melbourne. We thank CAHM and Research Laboratory Support Services and acknowledge support to them by the Peter MacCallum Cancer Foundation and the Australian Cancer Research Foundation. Open access publishing facilitated by The University of Melbourne, as part of the Wiley - The University of Melbourne agreement via the Council of Australian University Librarians.

Author contributions

Kellie Veen: Conceptualization; data curation; formal analysis; investigation; methodology; writing – original draft; writing – review and editing. **Phuong-Khanh Nguyen:** Data curation; formal analysis; investigation; methodology. **Francesca Froidi:** Data curation; formal analysis; supervision; investigation; methodology; writing – original draft; writing – review and editing. **Qian Dong:** Data curation; formal analysis; investigation. **Edel Alvarez-Ochoa:** Data curation; formal analysis; methodology. **Kieran F Harvey:** Writing – review and editing. **John PD McMullen:** Data curation; formal analysis;

investigation; methodology. **Owen Marshall:** Conceptualization; formal analysis; investigation; methodology; writing – original draft; project administration; writing – review and editing. **Patricia R Jusuf:** Supervision. **Louise Y Cheng:** Conceptualization; data curation; supervision; funding acquisition; writing – original draft; project administration; writing – review and editing.

Disclosure and competing interests statement

The authors declare that they have no conflict of interest.

References

- Abdusalamoglu MD, Eroglu E, Burkard TR, Knoblich JA (2019) The transcription factor odd-paired regulates temporal identity in transit-amplifying neural progenitors via an incoherent feed-forward loop. *Elife*8: e46566
- Apitz H, Salecker I (2014) A challenge of numbers and diversity: neurogenesis in the *Drosophila* optic lobe. *J Neurogenet*28: 233–249
- Aughey GN, Delandre C, McMullen JPD, Southall TD, Marshall OJ (2021) FlyORF-TaDa allows rapid generation of new lines for in vivo cell-type-specific profiling of protein–DNA interactions in *Drosophila melanogaster*. *G3 Genes, Genomes, Genetics*11: jkaa005
- Bayraktar OA, Doe CQ (2013) Combinatorial temporal patterning in progenitors expands neural diversity. *Nature*498: 1–8
- Bertet C, Li X, Erclik T, Cavey M, Wells B, Desplan C (2014) Temporal patterning of neuroblasts controls notch-mediated cell survival through regulation of hid or reaper. *Cell*158: 1173–1186
- Carney TD, Struck AJ, Doe CQ (2013) Midlife crisis encodes a conserved zinc-finger protein required to maintain neuronal differentiation in *Drosophila*. *Development*140: 4155–4164
- Cubenas-Potts C, Rowley MJ, Lyu X, Li G, Lei EP, Corces VG (2017) Different enhancer classes in *Drosophila* bind distinct architectural proteins and mediate unique chromatin interactions and 3D architecture. *Nucleic Acids Res*45: 1714–1730
- Delandre C, McMullen JP, Marshall OJ (2022) Membrane-bound fluorophore-labelled vectors for Targeted DamID allow simultaneous profiling of expression domains and DNA binding. *bioRxiv*<https://doi.org/10.1101/2020.04.17.045948> [PREPRINT]
- Egger B, Boone JQ, Stevens NR, Brand AH, Doe CQ (2007) Regulation of spindle orientation and neural stem cell fate in the *Drosophila* optic lobe. *Neural Dev*2: 1
- Eroglu E, Burkard TR, Jiang Y, Saini N, Homem CCF, Reichert H, Knoblich JA (2014) SWI/SNF complex prevents lineage reversion and induces temporal patterning in neural stem cells. *Cell*156: 1259–1273
- Friedmann-Morvinski D, Verma IM (2014) Dedifferentiation and reprogramming: origins of cancer stem cells. *EMBO Rep*15: 244–253
- Froidi F, Szuperak M, Weng C-F, Shi W, Papenfuss AT, Cheng LY (2015) The transcription factor Nerfin-1 prevents reversion of neurons into neural stem cells. *Genes Dev*29: 129–143
- Froidi F, Pachnis P, Szuperak M, Costas O, Fernando T, Gould AP, Cheng LY (2019) Histidine is selectively required for the growth of Myc-dependent dedifferentiation tumours in the *Drosophila* CNS. *EMBO J*38: e99895
- Gaultier C, Foppolo S, Maurange C (2022) Regulation of developmental hierarchy in *Drosophila* neural stem cell tumors by COMPASS and Polycomb complexes. *Sci Adv*8: eabi4529
- Genovese S, Clément R, Gaultier C, Besse F, Narbonne-Reveau K, Daian F, Foppolo S, Luis NM, Maurange C (2019) Coopted temporal patterning

- governs cellular hierarchy, heterogeneity and metabolism in *Drosophila* neuroblast tumors. *Elife*8: e50375
- Grosskortenhaus R, Pearson BJ, Marusich A, Doe CQ (2005) Regulation of temporal identity transitions in *Drosophila* neuroblasts. *Dev Cell*8: 193–202
- Harding K, White K (2018) *Drosophila* as a model for developmental biology: stem cell-fate decisions in the developing nervous system. *J Dev Biol*6: 25–22
- Hasegawa E, Kitada Y, Kaido M, Takayama R, Awasaki T, Tabata T, Sato M (2011) Concentric zones, cell migration and neuronal circuits in the *Drosophila* visual center. *Development*138: 983–993
- Jenett A, Rubin GM, Ngo T-TB, Shepherd D, Murphy C, Dionne H, Pfeiffer BD, Cavallaro A, Hall D, Jeter J et al (2012) A GAL4-driver line resource for *Drosophila* neurobiology. *Cell Rep*2: 991–1001
- Konstantinides N, Holguera I, Rossi AM, Escobar A, Dudragne L, Chen Y-C, Tran TN, Martínez Jaimes AM, Özel MN, Simon F et al (2022) A complete temporal transcription factor series in the fly visual system. *Nature*604: 316–322
- Li X, Erclik T, Bertet C, Chen Z, Voutev R, Venkatesh S, Morante J, Celik A, Desplan C (2013) Temporal patterning of *Drosophila* medulla neuroblasts controls neural fates. *Nature*498: 456–462
- Liu Z, Yang C-P, Sugino K, Fu C-C, Liu L-Y, Yao X, Lee LP, Lee T (2015) Opposing intrinsic temporal gradients guide neural stem cell production of varied neuronal fates. *Science*350: 317–320
- Magadi SS, Voutyraki C, Anagnostopoulos G, Zacharioudaki E, Poutakidou IK, Efraimoglou C, Stapountzi M, Theodorou V, Nikolaou C, Koumbanakis KA et al (2020) Dissecting Hes-centred transcriptional networks in neural stem cell maintenance and tumorigenesis in *Drosophila*. *Development*147: dev191544
- Marshall OJ, Brand AH (2015) damidseq_pipeline: an automated pipeline for processing DamID sequencing datasets. *Bioinformatics*31: 3371–3373
- Marshall OJ, Southall TD, Cheetham SW, Brand AH (2016) Cell-type-specific profiling of protein-DNA interactions without cell isolation using targeted DamID with next-generation sequencing. *Nat Protoc*11: 1586–1598
- Maurange C (2020) Temporal patterning in neural progenitors: from *Drosophila* development to childhood cancers. *Dis Model Mech*13: dmm044883
- Maurange C, Cheng L, Gould AP (2008) Temporal transcription factors and their targets schedule the end of neural proliferation in *Drosophila*. *Cell*133: 891–902
- Morante J, Desplan C (2008) The color-vision circuit in the medulla of *Drosophila*. *Curr Biol*18: 553–565
- Morante J, Erclik T, Desplan C (2011) Cell migration in *Drosophila* optic lobe neurons is controlled by *eyeless/Pax6*. *Development*138: 687–693
- Narbonne-Reveau K, Lanet E, Dillard C, Foppolo S, Chen C-H, Parrinello H, Rialle S, Sokol NS, Maurange C (2016) Neural stem cell-encoded temporal patterning delineates an early window of malignant susceptibility in *Drosophila*. *Elife*5: e13463
- Pahl MC, Doyle SE, Siegrist SE (2019) E93 integrates neuroblast intrinsic state with developmental time to terminate MB neurogenesis via autophagy. *Curr Biol*29: 750–762
- Ray A, Li X (2021) A Notch-dependent transcriptional mechanism controls expression of temporal patterning factors in *Drosophila* medulla. [bioRxiv](https://doi.org/10.1101/2021.10.29.466469)<https://doi.org/10.1101/2021.10.29.466469> [PREPRINT]
- Reichardt I, Bonnay F, Steinmann V, Loedige I, Burkard TR, Meister G, Knoblich JA (2018) The tumor suppressor *brat* controls neuronal stem cell lineages by inhibiting *deadpan* and *Zelda*. *EMBO Rep*19: 102–117
- Ren Q, Yang C-P, Liu Z, Sugino K, Mok K, He Y, Ito M, Nern A, Otsuna H, Lee T (2017) Stem cell-intrinsic, seven-up-triggered temporal factor gradients diversify intermediate neural progenitors. *Curr Biol*27: 1303–1313
- San-Juán BP, Baonza A (2011) The bHLH factor *deadpan* is a direct target of notch signaling and regulates neuroblast self-renewal in *Drosophila*. *Dev Biol*352: 70–82
- San-Juán BP, Andrade-Zapata I, Baonza A (2012) The bHLH factors *Dpn* and members of the E(spl) complex mediate the function of notch signalling regulating cell proliferation during wing disc development. *Biol Open*1: 667–676
- Southall TD, Gold KS, Egger B, Davidson CM, Caygill EE, Marshall OJ, Brand AH (2013) Cell-type-specific profiling of gene expression and chromatin binding without cell isolation: assaying RNA pol II occupancy in neural stem cells. *Dev Cell*26: 101–112
- Southall TD, Davidson CM, Miller C, Carr A, Brand AH (2014) Dedifferentiation of neurons precedes tumor formation in *Lola* mutants. *Dev Cell*28: 685–696
- Suzuki T, Kaido M, Takayama R, Sato M (2013) A temporal mechanism that produces neuronal diversity in the *Drosophila* visual center. *Dev Biol*380: 12–24
- Syed MH, Mark B, Doe CQ (2017) Steroid hormone induction of temporal gene expression in *Drosophila* brain neuroblasts generates neuronal and glial diversity. *Elife*6: e26287
- Tang JLY, Hakes AE, Krautz R, Suzuki T, Contreras EG, Fox PM, Brand AH (2022) NanoDam identifies Homeobrain (ARX) and scarecrow (NKX2.1) as conserved temporal factors in the *Drosophila* central brain and visual system. *Dev Cell*57: 1193–1207
- Tarazona S, Furió-Tarí P, Turrà D, Pietro AD, Nueda MJ, Ferrer A, Conesa A (2015) Data quality aware analysis of differential expression in RNA-seq with NOISeq R/bioc package. *Nucleic Acids Res*43: e140
- van den Ameele J, Brand AH (2019) Neural stem cell temporal patterning and brain tumour growth rely on oxidative phosphorylation. *Elife*8: e47887
- Vissers JHA, Foldi F, Schröder J, Papenfuss AT, Cheng LY, Harvey KF (2018) The scalloped and Nerfin-1 transcription factors cooperate to maintain neuronal cell fate. *Cell Rep*25: 1561–1576
- Xu J, Hao X, Yin M-X, Lu Y, Jin Y, Xu J, Ge L, Wu W, Ho M, Yang Y et al (2017) Prevention of medulla neuron dedifferentiation by Nerfin-1 requires inhibition of notch activity. *Development*144: 1510–1517
- Yasugi T, Umetsu D, Murakami S, Sato M, Tabata T (2008) *Drosophila* optic lobe neuroblasts triggered by a wave of proneural gene expression that is negatively regulated by JAK/STAT. *Development*135: 1471–1480
- Zhu H, Zhao SD, Ray A, Zhang Y, Li X (2021) A comprehensive temporal patterning gene network in *Drosophila* medulla neuroblasts revealed by single-cell RNA sequencing. [bioRxiv](https://doi.org/10.1101/2021.06.12.448145)<https://doi.org/10.1101/2021.06.12.448145> [PREPRINT]
- Zhu H, Zhao SD, Ray A, Zhang Y, Li X (2022) A comprehensive temporal patterning gene network in *Drosophila* medulla neuroblasts revealed by single-cell RNA sequencing. *Nat Commun*13: 1247



License: This is an open access article under the terms of the [Creative Commons Attribution](https://creativecommons.org/licenses/by/4.0/) License, which permits use, distribution and reproduction in any medium, provided the original work is properly cited